NACA TN 2408 8088

TECH LIBRARY KAFB, NM
0065695

NATIONAL ADVISORY COMMITTEE FOR AERONAUTICS

TECHNICAL NOTE 2408

APPROXIMATE DESIGN METHOD FOR HIGH-SOLIDITY BLADE ELEMENTS IN COMPRESSORS AND TURBINES

By John D. Stanitz

Lewis Flight Propulsion Laboratory
Cleveland, Ohio

Washington
July 1951

AFMDC
TECHNICAL LIBRARY
AFL 2811

TECH LIBRARY KAFB, NM
0065695

NATIONAL ADVISORY COMMITTEE FOR AERONAUTIC

TECHNICAL NOTE 2408

APPROXIMATE DESIGN METHOD FOR HIGH-SOLIDITY BLADE ELEMENTS IN COMPRESSORS AND TURBINES

By John D. Stanitz

SUMMARY

An approximate blade-element design method is developed for compressible or incompressible nonviscous flow in high-solidity stators or rotors of axial-, radial-, or mixed-flow compressors, turbines, or two-dimensional cascades. The method is based upon channel-type flow between blade elements on a specified surface of revolution that lies between the hub and shroud (casing) and is concentric with the axis of the compressor or turbine. The blade element is designed for prescribed velocities along the blade-element profile as a function of distance along meridional lines on the surface of revolution. The method is limited, because of assumptions, to prescribed velocities that result in blade-element profiles with gradual variations in thickness and with minimum radii of curvature at least approximately equal to the channel width between profiles.

Two numerical examples are presented: The first example is the design of a blade-element profile for a plane two-dimensional cascade in compressible flow with prescribed velocities along the profile; the second example is the design of a blade element for the impeller of a mixed-flow centrifugal compressor. In both examples the design method has been checked by comparing the prescribed velocity distribution with the velocity distribution obtained by stream-filament methods from the resulting blade-element design.

INTRODUCTION

Most aerodynamic losses in compressors and turbines result from the viscosity and compressibility of the fluid. (Other losses, for example, are associated with the trailing vortex sheet that sheds from the trailing edge of the blade if the circulation around the blade elements varies along the span of the blade.) Because the fluid is viscous, losses result from boundary-layer friction and separation and from secondary flows associated with the boundary layer. The magnitude of these losses depends on the boundary-layer thickness, the size of

which is controlled by the velocity distribution just outside the boundary layer. In particular, if the velocity decelerates too rapidly, the boundary layer thickens and separates, causing large mixing losses. Also, because the fluid is compressible, significant shock losses result if the maximum relative velocity on the blade surfaces appreciably exceeds the local speed of sound. In addition, if the relative velocity exceeds the local speed of sound for too great a distance across the channel between blades, "choke-flow" conditions develop and the blade row cannot pass the desired quantity of fluid. By proper selection of the velocity distribution relative to the blade surfaces, secondary-flow losses and boundary-layer friction and separation losses can be reduced, and shock losses and choke-flow conditions can be eliminated. With the assumption that desirable velocity distributions can be determined from boundary-layer theory and so forth, the problem of efficient compressor and turbine design is resolved into the development of design methods for blades that have prescribed velocity distributions.

In the past, a number of design methods have been developed for plane, two-dimensional cascades with prescribed velocities along the blade surfaces for incompressible flow (references 1 to 3, for example) and for compressible flow (references 4 and 5). These cascades are limited in application to axial-flow compressors and turbines. A method (reference 6) has also been developed for the design of radial-flow centrifugal impellers for incompressible flow and for a prescribed variation in work input with radius. Recently, work has been done (references 7 and 8, for example) on the general problem of blade design for mixed-flow compressors or turbines in which various independent variables are prescribed, but usually the relative velocity along the blade surfaces is not.

The work presented herein is concerned with an approximate design method developed at the NACA Lewis laboratory for blade elements with prescribed velocities along the profile. The method is developed for elements of high-solidity blades in compressors and turbines or for plane, two-dimensional cascades. The blade-element profile lies on a specified surface of revolution that is concentric with the axis of the compressor or turbine and lies on or between the hub and shroud (casing). The blade-element-design method is for compressible, nonviscous fluids and, because of assumptions required by the method, is limited to prescribed velocities that result in blade-element profiles with gradual variations in thickness and with minimum radii of curvature at least approximately equal to the channel width between profiles. (The nose and tail regions of the blade-element profile are excluded from the approximate blade-element-design method of this report.)

THEORY OF DESIGN METHOD

The approximate blade-element-design method is developed in two parts. The first part, called the first approximation, is simple and rapid and appears to be satisfactory for very high-solidity blades, such as exist in radial- and mixed-flow centrifugal compressors. The second part, called the second approximation, improves on the assumptions of the first part and appears to be satisfactory for blade solidities such as exist in present-day turbine nozzles.

Preliminary Considerations

Analysis problem. - In the aerodynamic theory of compressors and turbines there are two types of problem: first, the direct or analysis problem in which the velocities are determined for a given blade shape; and second, the inverse or design problem in which the blade shape is determined for prescribed velocities along the blade surfaces. It is the inverse or design problem with which this report is concerned, but by way of introduction to the design method the direct or analysis problem will be discussed first.

One possible means of analyzing the flow through a blade row (stator or rotor) with specified geometry is as follows: Consider the flow of an ideal, compressible fluid through an arbitrary channel between blades, such as shown in figure 1. The fluid is free to follow whatever path the pressure and inertia forces require of it. If, however, the number of blades in the blade row approaches infinity, the space between blades approaches zero and the path of the fluid is restricted to the curved, mean surface of the blade. (The blades become very thin so that the two surfaces of each blade approach a mean surface.) Under this assumption of axial symmetry (references 7 and 9, for example) the fluid flow is reduced from three-dimensional motion in the passage between blades with finite spacing to two-dimensional motion on the curved, mean blade surface. The streamlines of this two-dimensional motion can be projected on the meridional plane (axial-radial plane) as shown in figure 2. Ruden (reference 10) has shown that, provided the blades are not too widely spaced, axial-symmetry solutions give a good picture of the mean flow between blades.

For finite blade spacing, flow conditions vary from blade to blade (circumferentially about the axis of the compressor or turbine) as well as from hub to shroud. In order to investigate the variation from blade to blade, it is assumed that the motion of any fluid particle bounded by adjacent streamlines in the meridional plane (fig. 2) is restricted to the annulus generated by rotating these adjacent

streamlines about the axis of the compressor or turbine. If the adjacent streamlines are sufficiently close together, flow conditions in the annulus can be considered uniform normal to the mean surface of revolution within the annulus. Thus the fluid motion is reduced to two-dimensional flow on the mean surface of revolution (fig. 3) generated by rotating the center line between the adjacent streamlines in the meridional plane (fig. 2) about the axis of the compressor or turbine. Blade-to-blade solutions of this type are given in references 11 and 12.

Blade-to-blade solutions can be obtained for every mean surface of revolution generated by the center lines between adjacent streamlines in the meridional plane (fig. 2). Therefore, flow conditions can be determined approximately throughout the passage. The resulting quasi three-dimensional solution of the direct or analysis problem was obtained by the combination of two types of two-dimensional solution; axial-symmetry solutions in the meridional plane and blade-to-blade solutions on surfaces of revolution. Such a combination of solutions prohibits the possibility of a corkscrew path, which the fluid might follow in an exact three-dimensional solution, but it can be expected to give a better picture of the flow than does any two-dimensional solution alone.

Design problem. - It is proposed to solve the inverse or design problem by an approach similar, but reversed, to that outlined for the direct or analysis problem in the previous section. First, the profile of the blade element on one surface of revolution (fig. 3) will be determined for prescribed velocities along the profile. In order to accomplish this first phase of the blade-design method, the shape of the surface of revolution (fig. 3) is specified together with the variation in height of the fluid particles (or blade element) along the surface. The specified surface of revolution is generated by a prescribed curve that is the center line between two adjacent streamlines in the meridional plane. (The curve should be smooth with large radii of curvature, but is otherwise assumed arbitrary in shape.) The specified variation in height of the fluid particles (or blade element) along the surface of revolution is given by the prescribed spacing of the adjacent meridional streamlines that generate the annulus around the surface of revolution. (The variation in meridional streamline spacing along the center line should be smooth and slowly varying but is otherwise assumed arbitrary.)

After the profile of the blade element on the surface of revolution has been determined by design methods that will be developed in this report, the shape of the blade surfaces that cut through the profile of the blade element on the surface of revolution must be obtained and the hub and shroud contours of the blade in the meridional plane must be determined. A suggested method to accomplish this second phase of the design method (not the subject of this report) is first to prescribe the blade surfaces. (These surfaces

pass through the blade-element profile on the specified surface of revolution and extend to the hub and shroud casings, which are as yet undetermined. The prescribed shape of the blade surfaces determines the blade taper and the thickness distribution everywhere except on the specified surface of revolution.) The hub and shroud profiles are then determined by a solution to the inverse or design problem in the meridional (axial-radial) plane starting from the specified shape of the center line between adjacent streamlines in the meridional plane and the specified spacing between the adjacent streamlines and solving for the variation in meridional stream function outward and inward along normals to the meridional streamlines until the meridional streamlines along the root and tip (hub and shroud) of the blade are determined.

The specified spacing of the adjacent streamlines together with the known blade-element-profile thickness distribution determines the variation in meridional velocity along the specified center line between the streamlines. This arbitrary specification of the magnitude of the velocity along a specified stream path (the center line) overdetermines the problem and leads to singularities in the flow field. If, however, the prescribed velocity is reasonably consistent with the prescribed shape of the center line and if the velocity is prescribed along the center line at a finite number of points only, the hub and shroud (casing) can be determined (second phase of blade-design method) by finite-difference methods that in general are not troubled by the singularities. The resulting hub and shroud contours can be checked by a direct solution for the shape of the streamline corresponding to the prescribed center line and for the spacing of the adjacent streamlines. If the agreement with the prescribed center line and spacing of the adjacent streamlines is not good, either a new center line or a new meridional velocity distribution (spacing of the adjacent streamlines) or both are prescribed and the entire blade-design method is repeated until satisfactory agreement is achieved.

Thus the entire blade geometry can be determined for specified velocities along the profile of a blade element on one surface of revolution, which surface is specified together with the arbitrary (but smooth) variation in height of the fluid particles (or blade element) along the surface. Only the first phase of the proposed blade-design method will be considered in this report; that is, only the profile of a blade element on one surface of revolution will be determined for prescribed velocities along the blade profile. If the hub-shroud (root-tip) ratio of the blade is sufficiently large and if the specified shape of the center line between meridional streamlines has sufficiently small curvature, the second phase of the design method can be neglected, as is customarily done in the application of plane, two-dimensional cascade data to the design of axial-flow compressors and turbines, for example.

Coordinates. - The cylindrical coordinates R, θ, and Z are shown in figure 3. (All symbols are defined in appendix A.) These coordinates are dimensionless, the linear coordinates R and Z having been divided by a characteristic length equal to the chord c of the blade element (the exact definition of c will be given later). The coordinate system is oriented with its Z-axis along the axis of the compressor or turbine. The coordinates are fixed relative to the blades so that the coordinate system is absolute if the blades are stationary (stators) and relative if the blades are rotating (rotors). The angular velocity ω for rotors is always positive (right-hand rule) about the Z-axis, as shown in figure 3.

An elemental distance dS in the direction of flow (that is, coinciding with the velocity vector) has components dR, $Rd\theta$, and dZ (fig. 3). The projection of dS on the meridional plane is given by dM in figure 3. The elemental distances dS and dM help to define two angles α and β, where, from figure 3,

$$dR = dM \sin \alpha \tag{1a}$$

$$dZ = dM \cos \alpha \tag{1b}$$

and

$$dM = dS \cos \beta \tag{2a}$$

$$Rd\theta = dS \sin \beta \tag{2b}$$

Because dS and dM are always positive and finite, equation (2a) requires that

$$\frac{-\pi}{2} < \beta < \frac{\pi}{2}$$

From equation (2b) and figure 3, $\beta > 0$ for positive values of $Rd\theta$, and $\beta < 0$ for negative values of $Rd\theta$. Because both dS and dM lie on the surface of revolution, the angle β is the flow direction measured on this surface and is positive to the right when the exterior of the surface is viewed in the direction of dM (fig. 3).

In general, dZ can have both positive and negative values. In any blade row of most compressors and turbines, however, dZ will always have the same sign, which in this report shall be considered positive (or zero), so that from equation (1b),

$$\frac{-\pi}{2} \leq \alpha \leq \frac{\pi}{2}$$

For inflow machines (fig. 4(a)), dR is negative in the direction of dM and for outflow machines (fig. 4(b)), dR is positive, so that from equation (1a),

$$\frac{-\pi}{2} \leq \alpha < 0 \quad \text{(inflow machine)}$$

$$0 < \alpha \leq \frac{\pi}{2} \quad \text{(outflow machine)}$$

For axial-flow machines, dR approaches 0 so that, from equation (1a), α is approximately 0.

Velocity components. - The velocity Q relative to the coordinate system has components Q_R, Q_θ, and Q_Z in the R-, θ-, and Z-directions, respectively (fig. 3). These velocities are dimensionless, having been divided by a characteristic velocity equal to the absolute stagnation speed of sound a_o upstream of the blade row, where

$$a_o^2 = \gamma g R T_o \tag{3}$$

in which R is the gas constant, γ is the ratio of specific heats, g is the acceleration due to gravity, T is the static (stream) temperature, and the subscript o indicates stagnation conditions upstream of the blade row. For rotors, the tip speed of a blade element U_T is likewise dimensionless and is defined by

$$U_T = \frac{\omega R_T c}{a_o} \tag{4}$$

Thus, if

$$R^* = \frac{R}{R_T} \tag{5}$$

the tangential velocity of the blade at any radius R is equal to $R^* U_T$ and the absolute tangential velocity of the fluid is equal to $(R^* U_T + Q_\theta)$. For stator blades, ω is zero and therefore U_T is zero.

In addition to the three components of the relative velocity Q_R, Q_θ, and Q_Z, it is convenient to define a fourth velocity component, lying in the meridional plane and defined as the meridional velocity Q_M, where from figure 3,

$$Q_M = Q \cos \beta \tag{6a}$$

Also from figure 3,

$$Q_R = Q_M \sin \alpha \tag{6b}$$

$$Q_\theta = Q \sin \beta \tag{6c}$$

and

$$Q_Z = Q_M \cos \alpha \tag{6d}$$

Fluid particle. - As shown in figure 5, a fluid particle on a surface of revolution has the dimensions $Rd\theta$, dM, and ΔH. The differential angle $d\theta$ is measured in a plane normal to the Z-axis (fig. 5) and the differential distance dM is related to the differential radius dR by

$$dM = \frac{dR}{\sin \alpha} \tag{1a}$$

The incremental height ΔH (figs. 2 and 5) is measured normal to the surface of revolution and is determined by the specified spacing of the adjacent streamlines in the meridional plane (fig. 2). The incremental height ΔH is dimensionless, having been divided by the characteristic length c. The height ratio H^* of the fluid particle (fig. 5) is defined as the ratio of the incremental height ΔH of the blade element at radius R to the incremental height $(\Delta H)_T$ of the blade element at R_T.

Thermodynamic relations. - From the general energy equation, the static (stream) temperature can be shown to be related to the relative velocity Q by (reference 11)

$$\frac{T}{T_o} = 1 + \frac{\gamma-1}{2}\left[(R^* U_T)^2 - Q^2 - 2U_T \lambda_U\right] \tag{7}$$

where the subscript U refers to conditions upstream of the blade row and where λ is the whirl ratio (absolute moment of momentum divided by $cR_T a_o$) given by

$$\lambda = R^*(R^* U_T + Q_\theta) \tag{8}$$

The pressure ratio P and the density ratio ρ/ρ_o are likewise related to the relative velocity Q by

$$P = \frac{p}{p_o} = \left(\frac{T}{T_o}\right)^{\frac{\gamma}{\gamma-1}} = \left\{1 + \frac{\gamma-1}{2}\left[(R^* U_T)^2 - Q^2 - 2U_T\,\lambda_U\right]\right\}^{\frac{\gamma}{\gamma-1}} \tag{9}$$

and

$$\frac{\rho}{\rho_o} = \left(\frac{T}{T_o}\right)^{\frac{1}{\gamma-1}} = \left\{1 + \frac{\gamma-1}{2}\left[(R^* U_T)^2 - Q^2 - 2U_T\,\lambda_U\right]\right\}^{\frac{1}{\gamma-1}} \tag{10}$$

First Approximation

The first approximation gives a rapid means of computing the blade-element profile on any specified surface of revolution (with specified variation in H^*) for prescribed velocities along the profile. The method is based upon one-dimensional, channel-type flow between blade elements.

Assumptions. - For the first approximation, it is assumed that on the surface of revolution in the direction of θ (that is, for a given value of M) flow conditions may be considered uniform and equal to mass-weighted average values. This assumption is usual for one-dimensional, channel-type analyses, except that conditions have been considered uniform in the direction of θ rather than along a line normal to the average direction of flow. In particular, it is assumed that at a given value of M: (1) The mass-weighted average flow direction is equal to the direction of the blade-element camber line, and (2) the mass-weighted average velocity is equal to one-half the sum of the prescribed velocities at the two blade-element surfaces. Assumption (1) is approximately true for high-solidity blade elements with gradual

variations in profile thickness and is exactly true for infinite solidities. Assumption (2) is approximately true if the velocity distribution across the channel in the θ-direction is linear, a condition that is approached for high-solidity blade-element profiles with minimum radii of curvature at least approximately equal to the channel width between profiles (see fig. 15 of reference 11 and figs. 7 and 16 of reference 13).

Flow field. - A view on the θM-plane of the passage between two blade-element profiles is shown in figure 6. The flow field considered by the blade-element-design method lies between the profiles of the blade elements and between two parallel lines normal to the direction of Q_M and located close to the leading and trailing edges of the blades, as shown in figure 6. The immediate nose and tail regions have been excluded from the flow field considered by the blade-element-design method, because the small radii of curvature along the blade-element profile in these regions result in distributions of velocity and flow direction circumferentially across the channel between blade elements that do not satisfy the assumptions of the design method in these regions. In the final design, the nose and tail contours are rounded off in a manner guided by experience.

By definition, the characteristic length c (blade chord) is equal to the distance (not dimensionless) between the n- and t-boundaries (fig. 6) along a meridional line. Thus, the meridional distance M (dimensionless) when measured from the n-boundary is equal to 1.0 at the t-boundary.

The blade solidity σ is defined by

$$\sigma = \frac{1}{R_T(\Delta\theta)} \tag{11}$$

which, from figure 6, is the ratio of the blade chord c to the blade spacing at the tip of the blade element $cR_T(\Delta\theta)$ where $(\Delta\theta)$ is the angular spacing of the blades.

The ratio of channel width $R(\theta_1-\theta_0)$ to blade spacing $R(\Delta\theta)$ at a given value of M is defined by

$$\delta = \frac{\theta_1-\theta_0}{\Delta\theta} \tag{12}$$

where the subscripts 0 and 1 refer to the blade surfaces at the left and right of the channel walls, respectively, when viewed in the direction of Q_M. Thus, from equations (5), (11), and (12), the blade spacing (fig. 6) at a given value of M is equal to R^*/σ and the channel width is equal to $\delta R^*/\sigma$.

Prescribed velocities along blade-element contour. - In the proposed design method, the velocities Q_0 and Q_1 along the blade-element profile on the surface of revolution are prescribed as functions of M.

Outline of method. - The object of the design method is to determine the blade-element profile (on a specified surface of revolution with specified variations in H^*) for prescribed velocities along the blade-element contour and for prescribed flow conditions (whirl ratio and flow rate) upstream and downstream of the blade-element row. An inspection of figure 6 shows that the blade-element profile is completely described by the solidity σ and by

$$\delta = \delta(M) \tag{13}$$

and

$$\beta = \beta(M) \tag{14}$$

These quantities σ, δ, and β can be determined (approximately) from the prescribed velocities Q_0 and Q_1 and from the prescribed upstream and downstream conditions in a manner outlined as follows: (a) The solidity σ is determined by the blade-element spacing, which, for a given flow rate, depends on the specified change in whirl ratio upstream and downstream of the blade-element row and on the total blade-element torque; (b) the flow direction β at each value of M is obtained by equation (6c) from the average values of Q and Q_θ. The average value of Q is by assumption equal to one-half the sum of Q_0 and Q_1. The average value of Q_θ at M is determined by the blade-element torque between $M = 0$ and M; and (c) the ratio δ is determined from continuity considerations.

Solidity σ. - The blade-element solidity is determined from the condition that the rate of change of moment of momentum of the fluid flow between two blade elements must equal the torque of the blade elements on the fluid. For a fluid strip of width $c\,dM$ between blades (fig. 7) the torque of the blade elements is given by

$$- \left[p_o(\Delta P)\right] \quad \left[c(\Delta H)_T\, H^*\right] \quad \left[cR\right] \quad \left[c(dM)\right] \tag{15}$$

where

$$\Delta P = P_1 - P_0 \tag{16}$$

in which P is determined from equation (9) and from the specified velocities Q_1 and Q_0.

The rate of change of moment of momentum of the fluid flow across the strip in figure 7 is given by

$$cR_T a_o \frac{\Delta w}{bg} \frac{d\lambda_{av}}{dM}\, dM \tag{17}$$

where b is the number of blade elements (or passages between blade elements), $\frac{\Delta w}{b}$ is the incremental flow rate across the fluid strip (fig. 7) so that Δw is the total incremental flow rate along the surface of revolution, and the subscript av refers to the mass-weighted average value in the circumferential direction across the channel between blade elements at a given value of M.

Equating the quantities given by (15) and (17) and introducing the perfect gas law $(p = \rho RT)$ give

$$\frac{d\lambda_{av}}{dM} = \frac{-\sigma}{\gamma\varphi} H^* R^*\, \Delta P \tag{18}$$

where the flow coefficient φ is defined by

$$\varphi = \frac{1}{\rho_o a_o} \frac{\Delta w}{(\Delta f)_T} \tag{19}$$

where $(\Delta f)_T$, the total (blocked plus unblocked) incremental annulus area normal to the direction of Q_M at the blade-element tip, is given by

$$(\Delta f)_T = \left[b(\Delta\theta)\right] \quad \left[cR_T\right] \quad \left[c(\Delta H)_T\right] \tag{20}$$

Thus $\Delta w/(\Delta f)_T$ in equation (19) is the flow rate per unit total area at the blade-element tip.

The whirl ratio λ_{av} varies from λ_U to λ_D as M varies from 0 to 1.0 so that equation (18) integrates to give

$$\sigma = \frac{-\gamma\varphi(\lambda_D - \lambda_U)}{\int_0^1 H^*R^* \ (\Delta P) \ dM} \tag{21}$$

where H^*, R^*, and ΔP are known functions of M so that σ is directly determined by equation (21).

Average relative tangential velocity $(Q_\theta)_{av}$. - The mass-weighted average relative tangential velocity at any specified value of M is obtained by integrating equation (18) from $M = 0$ to M so that

$$\lambda_{av} - \lambda_U = -\frac{\sigma}{\gamma\varphi}\int_0^M H^*R^* \ (\Delta P) \ dM$$

which, from equation (8), becomes

$$(Q_\theta)_{av} = \frac{\lambda_U}{R^*} - R^*U_T - \frac{\sigma}{\gamma\varphi R^*}\int_0^M H^*R^* \ (\Delta P) \ dM \tag{22}$$

where σ is known from equation (21) so that $(Q_\theta)_{av}$ is directly determined by equation (22).

Flow direction β. - From equation (6c) and from the assumption that Q and β may be considered constant for any given value of M in the direction of θ between blade elements on the surface of revolution,

$$\beta = \sin^{-1}\left[\frac{(Q_\theta)_{av}}{Q_{av}}\right] \tag{23}$$

where, as already stated under the assumptions, the average value of Q is

$$Q_{av} = \frac{Q_0 + Q_1}{2} \tag{24}$$

Equations (22), (23), and (24) determine the flow direction β as a function of M.

Channel-width ratio δ. - The channel-width ratio is determined by continuity considerations. The incremental flow rate $\Delta w/b$ across the fluid strip in figure 7 is given by

$$\frac{\Delta w}{b} = \left[cR(\theta_1-\theta_0)\right] \quad \left[c(\Delta H)_T\, H^*\right] \quad \left[\rho_o \frac{\rho_{av}}{\rho_o}\right] \quad \left[a_o Q_{av}\right] \quad \cos\beta$$

from which, together with equations (12), (19), and (20),

$$\delta = \frac{\varphi}{R^*H^* \dfrac{\rho_{av}}{\rho_o} Q_{av} \cos\beta} \tag{25}$$

The ratio ρ_{av}/ρ_o is given by equation (10) with Q equal to Q_{av}. Equation (25) determines δ as a function of M. Upstream and downstream of the blade-element row, δ equals 1 so that from equation (25),

$$\varphi = \left(R^*H^* \frac{\rho}{\rho_o} Q \cos\beta\right)_U = \left(R^*H^* \frac{\rho}{\rho_o} Q \cos\beta\right)_D \tag{26}$$

which determines a relation that must be satisfied between $H^*R^* \dfrac{\rho}{\rho_o} Q \cos\beta$ upstream and downstream of the blade-element row.

Blade-element-profile coordinates. - The value of σ has been determined, and δ and β are known functions of M so that the design of the blade-element profile on the surface of revolution is complete (see equations (13) and (14)). The coordinates of the blade-element profile on the surface of revolution are obtained by (1) computing the shape of the profile camber line (fig. 6) on the surface of revolution, and (2) distributing the blade thickness equally on either side of the camber line.

The shape of the profile camber line is given by R and θ as functions of M. Because R (or R^*) is a known function of M, it only remains to determine $R\theta$ as a function of M in order to obtain the profile camber line. Along the camber line,

$$\frac{d(R\theta)}{dM} = R\frac{d\theta}{dM} + \theta\frac{dR}{dM}$$

which becomes, when combined with equations (1a), (2a), and (2b),

$$\frac{d(R\theta)}{dM} = \tan\beta + \theta\sin\alpha \tag{27}$$

The change in $R\theta$ from 0 at $M = 0$ to $R\theta$ at M is obtained by integrating equation (27) to yield

$$R\theta = \int_0^M (\tan\beta + \theta\sin\alpha)\,dM \tag{28}$$

Because R (or R^*) is a known (specified) function of M, equation (28) determines the blade-element camber line on the surface of revolution.

The blade thickness in the θ-direction is obtained from the channel-width ratio δ and is given by

$$R(\Delta\theta)\,(1-\delta) = \frac{R^*}{\sigma}\,(1-\delta) \tag{29}$$

This expression for the blade thickness is dimensionless, and is expressed, as usual, in units of characteristic length c. The blade thickness is equally distributed on either side of the camber line.

The blade-element spacing on the surface of revolution is given directly by the solidity σ.

Second Approximation

The second approximation modifies the results of the first approximation by estimating the variations in flow conditions in the θ-direction between blade elements on the surface of revolution.

Assumptions. - The major assumption of the second approximation is that, for high-solidity blade-element profiles with minimum radii of curvature at least approximately equal to the channel width between profiles (except at the nose and tail), flow conditions and products of flow conditions deviate only moderately (and smoothly) from a linear variation in the θ-direction across the channel between blade elements. Therefore, integrals involving the variation in the flow conditions (Q and β, for example) in the θ-direction can be evaluated by numerical methods using two-strip integration formulas (that is, assuming parabolic variations in the integrand).

In reference 13 it is shown that, for a high-solidity two-dimensional cascade with large turning angle and with a minimum radius of curvature along the blade-element profile (exclusive of the nose and tail) somewhat less than the channel width, the variations in Q, $Q \cos \beta$, and $Q \sin \beta$ can be represented in the θ-direction by a parabola. Also, for curved channels constructed from concentric streamlines of a potential vortex it is easily shown that, if the smaller radius of the channel walls is equal to the channel width, the velocity at midchannel is only 11 percent less than that given by a linear variation across the channel. Thus for this type of channel, if the minimum radius of curvature is at least approximately equal to the channel width, the velocity distribution deviates only moderately (and smoothly) from a linear variation and may therefore be represented by a parabola.

Flow field. - In the second approximation, the flow field on the surface of revolution is limited, as before, by the n- and t-boundaries (fig. 8). The flow direction β and the velocity Q vary in the θ-direction across the channel between blade elements, so that for constant M

$$\beta = \beta(X)$$

and

$$Q = Q(X)$$

where X indicates position across the channel in the θ-direction in percent of total distance between surfaces of adjacent blade elements (fig. 8)

$$X = \frac{\theta-\theta_0}{\theta_1-\theta_0} \tag{30}$$

Each streamline in the channel between blade elements is designated by the value of the stream function ψ along the streamline where, for convenience, the stream function is defined as the ratio of flow rate between the streamline and the left side of the channel, when viewed in the direction of Q_M, to total flow rate between blade elements. Thus, the 0-streamline, as indicated by the zero value of ψ, flows along the left channel wall (fig. 8); the 1.0-streamline flows along the right channel wall; and the 0.5-streamline equally divides the flow between blade elements. Numerical subscripts on β, X, and the velocity Q refer to the streamlines at which these quantities are considered. Thus, $\beta_{0.5}$ and $X_{0.5}$ refer to the values of β and X along the 0.5-streamline (fig. 8).

Outline of method. - An inspection of figure 8 shows that the blade-element profile on the specified surface of revolution (with specified variation in H^*) is completely described by the solidity σ and by

$$X_{0.5} = X_{0.5}(M) \tag{31}$$

$$\beta_{0.5} = \beta_{0.5}(M) \tag{32}$$

and

$$\delta = \delta(M) \tag{33}$$

These quantities (σ, $X_{0.5}$, $\beta_{0.5}$, and δ) can be determined (approximately) from the prescribed velocities Q_0 and Q_1 and from the prescribed upstream and downstream conditions in a manner outlined as follows:

(a) The solidity σ is the same as determined in the first approximation.

(b) The flow directions (approximate) on the blade surface β_0' and β_1' are obtained at arbitrarily specified values of M from the blade-element profile determined by the first approximation or by the previous cycle in the iteration calculations to be used in the second approximation. The superscript prime (') indicates values obtained from the first approximation or from the previous cycle in the iteration calculations.

(c) The ratio $X_{0.5}$ is approximately determined at specified values of M from continuity considerations using the prescribed values of Q_0 and Q_1 and the values of β_0' and β_1' obtained by (b).

(d) The velocity $Q_{0.5}$ at $X_{0.5}$ is estimated at specified values of M from considerations of absolute irrotational motion.

(e) The angle $\beta_{0.5}$ is approximately determined at specified values of M from the known value of $(Q_\theta)_{av}$ (equation (22)) assuming (see section Assumptions) that integrands consisting of the product of various flow conditions can be represented by parabolas that pass through known (or estimated) values of Q, β', and ρ/ρ_0 at X equal to 0, $X_{0.5}$, and 1.0.

(f) The channel-width ratio δ is approximately determined at specified values of M from continuity considerations assuming again that integrands consisting of the product of various flow conditions can be represented by a parabola.

(g) From the values obtained for $X_{0.5}$, $\beta_{0.5}$, and δ, a blade-element profile is determined so that new values for β_0' and β_1' can be obtained in (a) and the process repeated until the values of $X_{0.5}$, $\beta_{0.5}$, and δ converge.

Flow directions β_0' and β_1'. - In order to obtain the flow direction β_0' along the blade-element profile determined by the first approximation (or by the previous cycle in the iteration calculations of the second approximation), equation (30) is written

$$\theta_0' = \theta_{0.5}' - X_{0.5}' \left(\theta_1' - \theta_0'\right)$$

or, from equations (11) and (12),

$$\theta_0' = \theta_{0.5}' - X_{0.5}' \frac{\delta'}{R_T\sigma}$$

which, after differentiating with respect to M and multiplying by R, becomes

$$\tan \beta_0' = \tan \beta_{0.5}' - \frac{R^*}{\sigma} \frac{d(X_{0.5}' \delta')}{dM} \tag{34}$$

In like manner,

$$\tan \beta_1' = \tan \beta_{0.5}' + \frac{R^*}{\sigma} \frac{d\left[\left(1-X_{0.5}'\right) \delta'\right]}{dM} \tag{35}$$

Equations (34) and (35) determine β_0' and β_1'. For the first cycle in the second approximation, $X_{0.5}'$ is equal to 0.5 (equivalent to the assumption in the first approximation that the shape of the mean (0.5) streamline is the same as the blade-element camber line), and δ' and $\beta_{0.5}'$ are equal to δ and β from the first approximation. For succeeding cycles in the iteration calculations of the second approximation, $\beta_{0.5}'$, $X_{0.5}'$, and δ' are obtained from the preceding cycle.

Ratio $X_{0.5}$. - From the definition of the stream function ψ,

$$\psi = \frac{\int_0^X \frac{\rho}{\rho_o} Q \cos \beta \, dX}{\int_0^1 \frac{\rho}{\rho_o} Q \cos \beta \, dX} \tag{36}$$

For the 0.5-streamline, ψ equals 0.5 and X equals $X_{0.5}$, so that with β equal to β' equation (36) becomes

$$0.5 = \frac{\int_0^{X_{0.5}} \frac{\rho}{\rho_o} Q \cos \beta' \, dX}{\int_0^{1.0} \frac{\rho}{\rho_o} Q \cos \beta' \, dX} \tag{36a}$$

If the integrand $\left(\frac{\rho}{\rho_o} Q \cos \beta'\right)$ in equation (36a) deviates only moderately from a linear variation in the X-direction (see section Assumptions), it can be shown (appendix B) that, if a linear variation in the integrand is assumed in equation (36a), the value of $X_{0.5}$ obtained from equation (36a) is approximately equal to the value obtained by representing the integrand by a parabola. That is, for moderate deviations of the integrand from a linear variation, the value of $X_{0.5}$ depends more on the magnitude of the integrand at X equals 0 and 1.0 than on the magnitude of the deviation. If a linear variation in $\left(\frac{\rho}{\rho_o} Q \cos \beta'\right)$ with X is assumed, equation (36a) becomes

$$0.5 = \frac{k\, X_{0.5} + \frac{1}{2} X_{0.5}^{\,2}}{k + \frac{1}{2}}$$

or

$$X_{0.5} = -k \pm \sqrt{k^2 + k + \frac{1}{2}} \tag{37}$$

where

$$k = \frac{\left(\frac{\rho}{\rho_o} Q \cos \beta'\right)_0}{\left(\frac{\rho}{\rho_o} Q \cos \beta'\right)_1 - \left(\frac{\rho}{\rho_o} Q \cos \beta'\right)_0} \tag{37a}$$

The value of $X_{0.5}$ at each value of M is determined by equation (37). These values of $X_{0.5}$ can be used to compute new values of β_0' and β_1' by equations (34) and (35), and these new values of β_0' and β_1' result in new values of $X_{0.5}$ from equation (37). This iterative process converges rapidly and, in general, the second value of $X_{0.5}$ obtained from equation (37) is sufficiently accurate.

Velocity $Q_{0.5}$. - The velocity $Q_{0.5}$ is given by the following equation (obtained from equation (C8) in appendix C):

$$Q_{0.5} = \left[Q_0 + \frac{B}{A}\left(E + \frac{F}{A}\right) + \frac{C}{A}\right] \exp\left(A\, X_{0.5}\right) - \frac{B}{A}\left(E + \frac{F}{A} + F\, X_{0.5}\right) - \frac{C}{A} \tag{38}$$

where A is obtained by trial and error from

$$B = -\frac{\left[Q_1 - Q_0 \exp\left(A\right)\right] + C\left[\frac{1 - \exp\left(A\right)}{A}\right]}{\left(E + \frac{F}{A}\right)\left[\frac{1 - \exp\left(A\right)}{A}\right] + \frac{F}{A}} \tag{C9}$$

where

$$B = \frac{\delta'}{\sigma} R^* \cos \beta_{0.5}' \sin \beta_{0.5}' \tag{C6}$$

$$C = 2\,\frac{\delta'}{\sigma} R^* U_T \cos \beta_{0.5}' \frac{\sin \alpha}{R_T} \tag{C7}$$

$$E = \frac{dQ_0}{dM} \tag{C3a}$$

$$F = \frac{dQ_1}{dM} - \frac{dQ_0}{dM} \tag{C3b}$$

For small values of A, the numerical solutions of equations (38) and (C9) involve small differences of large numbers. In order to eliminate this condition, the equations can be expanded in the following series form:

$$Q_{0.5} = Q_0 \exp\left(A\, X_{0.5}\right) + BE\, X_{0.5} + C\, X_{0.5} +$$

$$(BEA + BF + CA)\left(\frac{X_{0.5}{}^2}{2!} + \frac{A\, X_{0.5}{}^3}{3!} + \frac{A^2\, X_{0.5}{}^4}{4!} + \ldots\right) \tag{38a}$$

and

$$B = \frac{\left[Q_1 - Q_0 \exp\left(A\right)\right] - C - CA\left(\frac{1}{2!} + \frac{A}{3!} + \frac{A^2}{4!} + \ldots\right)}{E + (EA + F)\left(\frac{1}{2!} + \frac{A}{3!} + \frac{A^2}{4!} + \ldots\right)} \tag{C9a}$$

in which forms the calculations are more easily carried out for small values of A.

Flow direction $\beta_{0.5}$. - At any position (X,M) in the channel between blade elements, the flow direction β (determined by the second approximation) is related to the uncorrected flow direction β' (determined by the blade-element profile of the first approximation, or by the profile of the previous cycle in the iteration calculations of the second approximation) by

$$\beta = \beta' + \Delta\beta \tag{39}$$

where $\Delta\beta$ is the correction added to β'. In general, for a given value of M, the correction $\Delta\beta$ varies with θ, but it can be shown (appendix D) that in the direction of θ, if $(\tan\beta - \tan\beta_{0.5})$ is small (a condition that is approached in high-solidity blades with gradual variations in blade-element-profile thickness) and if $\Delta\beta_{0.5}$ is small, then

$$\Delta\beta \approx \Delta\beta_{0.5}$$

The correction $\Delta\beta$ is therefore assumed constant across the channel between blade elements. Thus, for example, equation (39) becomes

$$\beta_{0.5} = \beta'_{0.5} + \Delta\beta \tag{40}$$

The correction $\Delta\beta$ is determined from considerations of the average relative tangential velocity, which is defined by

$$(Q_\theta)_{av} = \frac{\int_0^1 \frac{\rho}{\rho_o} Q^2 \sin\beta \cos\beta \, dX}{\int_0^1 \frac{\rho}{\rho_o} Q \cos\beta \, dX} \tag{41}$$

From equation (39) with $\Delta\beta$ assumed to be small,

$$\cos\beta \approx \cos\beta' - \Delta\beta \sin\beta' \tag{42a}$$

$$\sin\beta \approx \sin\beta' + \Delta\beta \cos\beta' \tag{42b}$$

and

$$\sin\beta \cos\beta \approx \frac{1}{2} \sin 2\beta' + \Delta\beta \cos 2\beta' \tag{42c}$$

From equations (41) and (42),

$$\Delta\beta = \frac{(Q_\theta)_{av}\int_0^1 \frac{\rho}{\rho_o} Q \cos\beta' \, dX - \frac{1}{2}\int_0^1 \frac{\rho}{\rho_o} Q^2 \sin 2\beta' \, dX}{\int_0^1 \frac{\rho}{\rho_o} Q^2 \cos 2\beta' \, dX + (Q_\theta)_{av}\int_0^1 \frac{\rho}{\rho_o} Q \sin\beta' \, dX} \tag{43}$$

Let I be any one of the integrands in equation (43); then if I varies in a parabolic manner (see section Assumptions) across the channel between blade elements,

$$I = e_a + e_b X + e_c X^2$$

so that

$$I_0 = e_a$$

$$I_{0.5} = e_a + e_b X_{0.5} + e_c X_{0.5}^2$$

and

$$I_1 = e_a + e_b + e_c$$

Therefore,

$$\int_0^1 I \, dX = \frac{1}{2}\left[I_0\left(\frac{3\,X_{0.5} - 1}{3\,X_{0.5}}\right) - I_{0.5}\left(\frac{1}{3\,X_{0.5}\,(X_{0.5} - 1)}\right) + I_1\left(\frac{3\,X_{0.5} - 2}{3\,X_{0.5} - 3}\right)\right] \tag{44}$$

(With $X_{0.5}$ equal to 0.5, equation (44) reduces to Simpson's one-third rule for numerical integration.)

The direction $\beta_{0.5}$ is therefore given by equation (40) in which $\Delta\beta$ is obtained from equation (43) where the integrals are determined by equation (44). (The values of Q, ρ/ρ_o, and β' contained in I_0, $I_{0.5}$, and I_1 of equation (44) are known. For the first cycle of the second approximation, $\beta'_{0.5}$ is equal to β obtained by the first approximation and for succeeding cycles of the second approximation, $\beta'_{0.5}$ is obtained from the preceding cycle.)

Channel-width ratio δ. - From continuity considerations of the fluid flow across the strip between channel walls in figure 7,

$$\frac{\Delta w}{b} = \left[cH^* \, (\Delta H)_T\right] (cR^* \, R_T) \int_{\theta_0}^{\theta_1} \rho_o \, a_o \, \frac{\rho}{\rho_o} \, Q \cos\beta \, d\theta$$

which, from equations (12), (19), (20), and (30), becomes

$$\varphi = \delta \, H^* R^* \int_0^1 \frac{\rho}{\rho_o} \, Q \cos\beta \, dX$$

or, from equations (39) and (42a),

$$\delta = \frac{\varphi}{H^*R^*\left[\int_0^1 \frac{\rho}{\rho_o} Q \cos \beta' \, dX - \Delta\beta \int_0^1 \frac{\rho}{\rho_o} Q \sin \beta' \, dX\right]} \tag{45}$$

Equation (45) determines the channel-width ratio. The integrals in equation (45) are given by equation (44).

The values of $\beta_{0.5}$ and δ obtained by the first cycle of the second approximation can be used to determine new values of β_0', β_1', $X_{0.5}$, and $Q_{0.5}$ from which new and presumably better values of $\beta_{0.5}$ and δ can be determined. This iterative process can be continued until the values of $\beta_{0.5}$ and δ converge. In general, the iterative process converges rapidly and, in many cases, only the first cycle of the second approximation is necessary.

Blade-element-profile coordinates. - The value of σ has been determined, and R^*, H^*, $X_{0.5}$, $\beta_{0.5}$, and δ are known functions of M so that the design of the blade element is complete. The coordinates of the blade-element profile on the surface of revolution are obtained as indicated in figure 8 by (1) computing the shape of the 0.5-streamline, which is obtained from $\beta_{0.5} = \beta_{0.5}(M)$, (2) distributing the channel width on either side of the 0.5-streamline according to $X_{0.5} = X_{0.5}(M)$, and (3) obtaining the blade profile from the channel shape and from the spacing of the channels, which spacing is determined by σ.

The shape of the 0.5-streamline is given by R and θ as functions of M. Because R (or R^*) is a known (specified) function of M, only $(R\theta)_{0.5}$ remains to be determined as a function of M. From equation (28), which assumes $R\theta$ is zero at $M = 0$,

$$(R\theta)_{0.5} = \int_0^M (\tan \beta_{0.5} + \theta \sin \alpha) \, dM \tag{46}$$

Equation (46), together with the specified variation in R, determines the shape of the 0.5-streamline on the surface of revolution.

The channel width is $\frac{\delta}{\sigma} R^*$ of which $X_{0.5} \frac{\delta}{\sigma} R^*$ is distributed to the left of the 0.5-streamline and $(1 - X_{0.5}) \frac{\delta}{\sigma} R^*$ is distributed to the right (when viewed in the direction of Q_M, fig. 8). The expression for the channel width is dimensionless and is expressed, as usual, in units of characteristic length c.

The blade-element profile results when the adjacent channel is placed with the spacing between 0.5-streamlines equal to R^*/σ (fig. 8). The blade-element profile is closed by rounding-off the nose and tail in a manner guided by experience.

APPLICATION OF DESIGN METHODS

The application of the first and second approximations of the blade-element-design method is considered in this section.

Types of blading. - The blade-element-design method developed in this report applies to compressible or incompressible flow in stators or rotors of radial-, axial-, or mixed-flow compressors, turbines, or two-dimensional cascades. The design of any particular blade element depends on which of the preceding categories describe the application of the blade element. Each category determines the magnitude or sign of various parameters that appear in the equations developed for the design method.

The blade element is first classified according to the compressibility of the fluid for which it was designed. For compressible fluids, the density ratio ρ/ρ_0 varies according to equation (10); for incompressible fluids, the density ratio is constant and equal to 1.

The blade element is next classified as a stator or rotor. For stators the angular velocity ω is zero so that the tip speed U_T is zero (equation (4)); for rotors the tip speed is positive. (Note that the angular velocity is always positive (right-hand rule) about the Z-axis (fig. 4).)

The blade element is next classified as inflow, axial flow, or outflow. For inflow blades (fig. 4(a)), the radius R decreases in the direction of M; thus from equation (1a) the angle α is less than zero. For axial-flow blades, α approaches zero. For outflow blades (fig. 4(b)), the radius R increases in the direction of M so that α is greater than zero.

The blade element is also classified as a compressor, turbine, or two-dimensional-cascade blade. In the case of rotor blades, Q_1 is greater than Q_0 for compressors, and Q_1 is less than Q_0 for turbines. For plane two-dimensional cascade blades, the surface of revolution becomes a flat plane, and

$$\left.\begin{aligned} H^* &= 1.0 \\ R^* &= 1.0 \\ \left.\begin{aligned} R &= \infty \\ d\theta &= 0 \end{aligned}\right\} & Rd\theta = dN \\ \alpha &= 0 \\ U_T &= 0 \end{aligned}\right\} \tag{47}$$

where N is the coordinate distance measured normal to M on the flat plane of the two-dimensional cascade.

Prescribed upstream and downstream flow conditions. - The designer of blade elements is generally given the upstream and downstream flow conditions for each blade element. These flow conditions are: (1) specified surface of revolution $R^* = R^*(M)$, (2) specified height ratio $H^* = H^*(M)$, (3) upstream and downstream whirl ratios λ_U and λ_D, and (4) the flow coefficient φ (equation (19)).

For axial-flow blade elements, R^* and H^* are considered constant upstream and downstream of the blade-element row so that the quantities Q_U, β_U, Q_D, and β_D are constant. It is therefore customary to specify any three of these quantities (instead of λ_U, λ_D, and φ); the fourth quantity is then determined from continuity considerations (equation (26)). For radial- or mixed-flow blade elements, however, R^* and H^* generally vary upstream and downstream of the blade-element row so that $(Q \text{ and } \beta)_U$ and $(Q \text{ and } \beta)_D$ vary and it is more convenient to specify the upstream and downstream conditions by the quantities λ_U, λ_D, and φ, which are always constant.

Prescribed velocities along blade-element profile. - In this blade-element-design method, the prescribed velocities Q_0 and Q_1 on the blade-element surfaces are specified as functions of the meridional coordinate M, rather than as functions of the arc length S, along

the blade-element profile. Any relation between Q_0 and Q_1 and M can be prescribed, but, if a physically acceptable blade-element profile is desired, and if gradual variations in blade-element-profile thickness together with a minimum radius of curvature at least approximately equal to the channel width is desired in order to satisfy the assumptions of the design method, the prescribed relation must exhibit the following features:

(1) In order to avoid negative blade thicknesses, which result when the channel width in the circumferential direction is greater than the blade spacing (that is, when $\delta > 1.0$), the average velocity Q_{av}, defined by

$$Q_{av} = \frac{1}{2}(Q_0 + Q_1) \tag{24}$$

must not be too low. As indicated by equation (25), the minimum allowable value of Q_{av} depends, among other things, on the value of β, which unfortunately is not known until the blade element has been designed.

(2) In order to obtain desirable blade-element thicknesses $\frac{R^*}{\sigma}(1-\delta)$ at the n- and t-boundaries (fig. 8, for example), the specified values of $(Q_{av})_n$ and $(Q_{av})_t$ must be approximately equal to the values given by equation (25) for specified values of δ and estimated (not yet known) values of β. These values of Q_{av} must be adjusted later if they result in undesirable blade-element thicknesses in the final calculations.

(3) In order to obtain a physically desirable rate of increase of blade thickness near the nose, $\left(\frac{dQ_{av}}{dM}\right)_n$ at $M = 0$ must have a suitable positive value, which is best determined from experience and which depends on the unknown solidity (to be determined), on the unknown variation in β with M (to be determined), and on the prescribed variation in R^*H^* with M. Likewise, to obtain a desirable rate of decrease of blade thickness near the tail, $\left(\frac{dQ_{av}}{dM}\right)_t$ at $M = 1.0$ must have a suitable low, perhaps negative, value, which also depends on the solidity and on the variation in β and R^*H^* with M.

(4) In order to obtain the fewest blades (that is, lowest solidity) possible, consistent with other requirements and limitations, it is desirable that the blade loading ΔQ, defined by

$$\Delta Q = Q_1 - Q_0 \tag{48}$$

be as large as possible over as great a range of M as possible. This fact is indicated by equation (21), because ΔP increases with ΔQ. Thus, it is generally desirable to prescribe blade loading even at the nose and tail (n- and t-boundaries, fig. 8). The blade is then assumed to load and unload over the regions that correspond to rounding-off of the nose and tail, respectively. The loading $(\Delta Q)_n$ and $(\Delta Q)_t$ must not, however, be too large; otherwise assumptions of the design method are violated. For example, if ΔQ is large in the vicinity of the nose or tail, this sudden loading or unloading of the blade can be expected to cause β, Q, and $\frac{dQ}{dM}$ to deviate greatly (and in a sudden manner) from a linear variation in the θ-direction (which deviation violates the assumption of the blade-element design method that the deviation is smooth and moderate). The maximum loading $(\Delta Q)_m$ should occur at some value of M between, but not close to, the nose and tail $(0 < M < 1.0)$.

(5) The prescribed variation in Q_0 and Q_1 with M should be smooth with gradual variations in $\frac{dQ_0}{dM}$ and $\frac{dQ_1}{dM}$. Sudden variations in $\frac{dQ_0}{dM}$ and $\frac{dQ_1}{dM}$ result in small radii of curvature locally on the blade-element profile (such as occur at the nose and tail, for example) and cause β, Q, and $\frac{dQ}{dM}$ to deviate greatly (and in a sudden manner) from a linear variation in the θ-direction.

One possible way of incorporating the preceding considerations in the prescribed distributions of Q_0 and Q_1 is given by

$$Q_0 = Q_{av} - \frac{\Delta Q}{2} \tag{49a}$$

$$Q_1 = Q_{av} + \frac{\Delta Q}{2} \tag{49b}$$

where

$$Q_{av} = d_a + d_b M + d_c M^2 + d_d M^3 \tag{50a}$$

and

$$\Delta Q = j_a + j_b M + j_c M^2 + j_d M^3 \tag{50b}$$

The coefficients d and j in equations (50a) and (50b) are obtained from the following conditions:

$$Q_{av} = (Q_{av})_n \quad \text{at} \quad M = 0$$

$$Q_{av} = (Q_{av})_t \quad \text{at} \quad M = 1.0$$

$$\frac{dQ_{av}}{dM} = \left(\frac{dQ_{av}}{dM}\right)_n \quad \text{at} \quad M = 0$$

$$\frac{dQ_{av}}{dM} = \left(\frac{dQ_{av}}{dM}\right)_t \quad \text{at} \quad M = 1$$

$$\Delta Q = (\Delta Q)_n \quad \text{at} \quad M = 0$$

$$\Delta Q = (\Delta Q)_t \quad \text{at} \quad M = 1$$

$$\Delta Q = (\Delta Q)_m \quad \text{at} \quad M = M_m$$

$$\frac{d(\Delta Q)}{dM} = 0 \quad \text{at} \quad M = M_m$$

so that

$$\left.\begin{aligned}
d_a &= (Q_{av})_n \\
d_b &= \left(\frac{dQ_{av}}{dM}\right)_n \\
d_c &= 3\left[(Q_{av})_t - (Q_{av})_n\right] - \left(\frac{dQ_{av}}{dM}\right)_t - 2\left(\frac{dQ_{av}}{dM}\right)_n \\
d_d &= \left(\frac{dQ_{av}}{dM}\right)_n + \left(\frac{dQ_{av}}{dM}\right)_t - 2\left[(Q_{av})_t - (Q_{av})_n\right]
\end{aligned}\right\} \tag{51}$$

and

$$\left.\begin{aligned}
j_a &= (\Delta Q)_n \\
j_b &= \frac{1}{M_m^2\,(1-M_m)^2}\Big[-(\Delta Q)_n\,(M_m^4 - 3M_m^2 + 2M_m) - \\
&\qquad (\Delta Q)_m\,(3M_m^2 - 2M_m) + (\Delta Q)_t\,(M_m^4)\Big] \\
j_c &= \frac{1}{M_m^2\,(1-M_m)^2}\Big[(\Delta Q)_n\,(2M_m^3 - 3M_m^2 + 1) + \\
&\qquad (\Delta Q)_m\,(3M_m^2 - 1) - (\Delta Q)_t\,(2M_m^3)\Big] \\
j_d &= \frac{1}{M_m^2\,(1-M_m)^2}\Big[-(\Delta Q)_n\,(M_m^2 - 2M_m + 1) - \\
&\qquad (\Delta Q)_m\,(2M_m - 1) + (\Delta Q)_t\,(M_m^2)\Big]
\end{aligned}\right\} \tag{52}$$

Equations (49a) and (49b) are a suggested means of prescribing satisfactory distributions of Q_0 and Q_1; any other method that results in acceptable blade-element profiles can be used.

Outline of numerical procedure. - The following outline of the numerical procedure includes both the first and second approximations. For convenience, the outline is divided into four parts: (I) Specified Conditions, (II) Preliminary Calculations, (III) First Approximation, and (IV) Second Approximation:

I - Specified Conditions

(1) Specify $R = R(Z)$, which determines the specified surface of revolution and from which is obtained the constant R_T and the relations

$$R^* = R^*(M)$$

and

$$\alpha = \alpha(M)$$

(2) Specify $H^* = H^*(M)$.

(3) Specify λ_U, λ_D, and φ, which determine the flow conditions upstream and downstream of the blade elements. (For axial-flow blade elements, it is customary to specify (instead) any three of the quantities Q_U, β_U, Q_D, and β_D; the fourth quantity is then determined by equation (26) in which $\frac{\rho}{\rho_0}$ is given by equation (10). The quantities λ_U, λ_D, and φ are then determined by equations (8) and (26)).

(4) Specify U_T, which is zero for stators.

(5) Specify $Q_0 = Q_0(M)$ and $Q_1 = Q_1(M)$.

(Use equations (49a) and (49b) or any other arbitrary method. These prescribed values of Q_0 and Q_1 may have to be adjusted later to result in physically acceptable blade-element profiles on the surface of revolution.)

II - Preliminary Calculations

(1) Compute ΔP as a function of M from equations (9) and (16).

(2) Compute the solidity σ from equation (21) by numerical integration.

(3) Compute number of blades b from

$$b = \frac{2\pi}{\Delta\theta} \tag{53}$$

where $\Delta\theta$ is obtained from equation (11). If the number of blades is not an integer, the solidity σ must be changed by adjusting any or all of φ, λ_D, λ_U, and $\int_0^1 H^*R^*(\Delta P)\,dM$, as indicated by equation (21).

(4) Compute $(Q_\theta)_{av}$ as a function of M from equation (22) by numerical integration.

III - First Approximation

(1) Compute Q_{av} as a function of M from equation (24).

(2) Compute β from equation (23).

(3) Compute δ from equation (25).

(If the coordinates of the blade-element profile on the surface of revolution are to be determined after the first approximation (that is, if the second approximation is not used), continue with the remaining steps in this section; otherwise proceed immediately from here to the next section.)

(4) The R,θ coordinates of the blade camber line on the surface of revolution are given by the specified relation between R (or R^*) and M, and by $R\theta$ as a function of M, which is obtained from equation (28) by numerical integration.

(5) The blade thickness in the circumferential direction is equally distributed on either side of the blade camber line and is given by equation (29).

(6) The angular blade spacing $\Delta\theta$ is obtained from the solidity, according to equation (11).

(7) The nose and tail of the blade are rounded off (fig. 6) in a manner guided by experience.

(8) For plane two-dimensional cascades the M,θ coordinates are replaced by M,N coordinates where dN replaced the product $Rd\theta$. The solidity σ, defined by equation (11), thus becomes equal to the reciprocal of the blade spacing (which spacing is expressed in units of the characteristic length c, so that the solidity is equal to the chord divided by the blade spacing).

IV - Second Approximation

The second approximation (part IV) follows after step (3) of the first approximation (part III).

(1) The angles β_0' and β_1' are obtained from equations (34) and (35) with $X_{0.5}$ assumed to equal 0.5, and with $\beta_{0.5}'$ and δ' equal to β and δ, respectively, from the first approximation.

(2) The ratio $X_{0.5}$ is obtained from equation (37).

(3) If desired, the angles β_0' and β_1' can be recomputed from equations (34) and (35) using $X_{0.5}$ from step (2). This iterative process can be continued, although the process generally converges rapidly enough so that only one step in addition to step (2) is necessary.

(4) Compute the corrected flow direction $\beta_{0.5}$ from equations (39) and (43). The integrals in equation (43) are evaluated by equation (44) in which the velocity $Q_{0.5}$ is given by equation (38) or (38a). To solve these equations initially, the values of $\beta_{0.5}'$ and δ' are the β and δ obtained by the first approximation.

(5) Compute the corrected channel-width ratio δ by equation (45).

(6) The corrected values of $\beta_{0.5}$ and δ are obtained initially from quantities that are based upon β and δ determined by the first approximation. If these quantities (β_0', β_1', $X_{0.5}$, and $Q_{0.5}$, for example) are recomputed using the corrected values of $\beta_{0.5}$ and δ, new, and presumably better, values of $\beta_{0.5}$ and δ are obtained. This iterative process can be continued until the values of $\beta_{0.5}$ and δ converge. In general, the process converges rapidly and, in many cases, only the first cycle of the second approximation is necessary.

(7) The shape of the 0.5-streamline on the surface of revolution is given by the specified relation between R (or R^*) and M, and by

$$(R\theta)_{0.5} = f(M)$$

which is obtained from equation (46) by numerical integration.

(8) The channel width $\frac{\delta}{\sigma} R^*$ is distributed on either side of the 0.5-streamline according to the ratio $X_{0.5}$, which is obtained from equation (37) using the final corrected values of $\beta_{0.5}$ and δ.

(9) The blade-element profile results when the adjacent channel is placed with the spacing between 0.5-streamlines equal to $\frac{R^*}{\sigma}$ (fig. 8).

(10) The blade-element profile is closed by rounding off the nose and tail in a manner guided by experience.

Boundary-layer corrections. - The blade profiles obtained by the first and second approximations are based upon the assumption of a non-viscous fluid. For real, viscous fluids a boundary layer, within which the viscosity cannot be neglected, builds up along the blade surfaces and displaces the potential flow. If the prescribed velocities for which the blade was designed do not have large enough decelerations to cause separation of the boundary layer, the thickness of the boundary layer can be corrected for, at least partially, by machining from the blade profile an amount equal to the displacement thickness of the boundary layer, which thickness can be estimated from boundary-layer theory.

NUMERICAL EXAMPLES

Two numerical examples are presented. The first example is for compressible flow between blade elements of a plane two-dimensional cascade with prescribed velocities along the blade-element profile. The second example is for compressible flow between blade elements of a mixed-flow impeller with prescribed velocities along the blade-element profile. In both examples, the design method has been checked by comparing the prescribed velocity distribution with the velocity distribution obtained by stream-filament methods on the resulting blade-element design.

First Numerical Example

The first numerical example is the design of a blade-element profile for a plane two-dimensional cascade that accelerates the fluid by turning it from β equals zero upstream of the cascade to β equals 60° downstream.

Prescribed conditions. - For any plane two-dimensional cascade the conditions given by equation (47) apply. Also, for the first numerical example the following flow conditions upstream and downstream of the cascade are given:

$$Q_D = 0.750$$

$$\beta_D = 60^{\circ}$$

$$\beta_U = 0^{\circ}$$

so that, from equation (26),

$$Q_U = 0.290$$

and

$$\varphi = 0.278$$

Prescribed velocity distribution. - The prescribed velocity distribution was determined by the following quantities, the magnitudes of which were based on considerations previously outlined in this report:

$$\left.\begin{aligned}(Q_{av})_n &= 0.348\\ (Q_{av})_t &= 0.751\end{aligned}\right\}\ \text{by trial and error to obtain satisfactory values for } \delta_n \text{ and } \delta_t$$

$$\left.\left(\frac{dQ_{av}}{dM}\right)_n = 0.444\right\}\ \text{chosen so that } \left(\frac{dQ_0}{dM}\right)_n = 0$$

$$\left(\frac{dQ_{av}}{dM}\right)_t = -\ 0.050$$

$$(\Delta Q)_n = 0.200$$

$$(\Delta Q)_t = 0.100$$

$$(\Delta Q)_m = 0.400$$

$$M_m = 0.450$$

so that, from equations (50a), (50b), (51), and (52),

$$Q_{av} = 0.348 + 0.444\ M + 0.371\ M^2 - 0.412\ M^3$$

$$\Delta Q = 0.200 + 0.888\ M - 0.984\ M^2 - 0.004\ M^3$$

from which Q_0 and Q_1 are obtained by equations (49a) and (49b). The velocity distribution is given in table I and is plotted in figure 9. (Sonic velocity occurs at Q equal to 0.915.) As a result of this velocity distribution the solidity σ is equal to 1.215 (from equation (21)). The pressure difference ΔP and the average relative tangential velocity $(Q_\theta)_{av}$ are tabulated as functions of M in table I.

Results. - The values of β and δ that determine the blade-element profile for the first approximation are given in table I together with the values of $\beta_{0.5}$, δ, and $X_{0.5}$ that determine the blade profile for the second approximation. The blade-element profile obtained by the second approximation is plotted in figure 10 together with the streamlines (obtained from equation (36)) and velocity potential lines used by the stream-filament method to estimate velocities along the blade-element profile. (The blade nose and tail are rounded off in an arbitrary manner.) The velocities obtained by the stream-filament method are compared in figure 9 with the prescribed velocities. The comparison is considered satisfactory, although the design method is not recommended for lower solidities.

The resulting blade-element profiles for the first and second approximations are compared in figure 11. The two profiles are significantly different and it is concluded that for blade-element solidities as low as that for the first numerical example ($\sigma = 1.215$), the second approximation is required.

Second Numerical Example

The second numerical example is the design of a blade-element profile for the impeller of a mixed-flow centrifugal compressor with prewhirl (λ_U) and with forward-curved blades at the impeller tip.

Surface of revolution. - For the mixed-flow impeller of the second numerical example, the surface of revolution is generated by rotating the circular arc shown in figure 12 about the axis of the impeller (Z-axis). At the blade-element nose (n-boundary)

$$\alpha_n = 0$$

$$R_n = 0.5\ R_T$$

and at the blade-element tail (t-boundary)

$$\alpha_t = 45^\circ$$

$$R_t = 1.0\ R_T$$

so that the circular arc subtends an angle of 45° and has a radius Y equal to 1.707 R_T. The length of the circular arc, or blade-element chord, is unity, so that (from fig. 12)

$$Y\frac{\pi}{4} = 1.0$$

from which R_T is equal to 0.746.

Transformed coordinates. - For convenience in the stream-filament check the following transformation of coordinates, which conformally transforms the surface of revolution into a flat plane, has been introduced:

$$dL^* = \frac{dL}{\Delta L} \tag{54a}$$

and

$$d\theta^* = \frac{d\theta}{\Delta L} \tag{54b}$$

where

$$dL = \frac{dM}{R} = \frac{dR}{R \sin \alpha} \tag{55a}$$

and

$$\Delta L = \int_{L_n}^{L_t} dL = \int_{R_n}^{R_t} \frac{dR}{R \sin \alpha} \tag{55b}$$

For the surface of revolution in the second numerical example,

$$\frac{1}{\sin \alpha} = \frac{Y}{\sqrt{Y^2 - (Y + R_n - R)^2}} \tag{56}$$

so that equation (55b) integrates to give

$$\Delta L = \frac{Y}{\sqrt{R_n (2Y + R_n)}} \left\{ \frac{\pi}{2} + \sin^{-1} \left[\frac{R_t (Y + R_n) - R_n (2Y + R_n)}{R_t Y} \right] \right\} = 2.096$$

Also, equation (54a), combined with equations (55a) and (56), integrates to give

$$L^* = \frac{\int_{R_n}^{R} \frac{dR}{R \sin \alpha}}{\Delta L} = \frac{\frac{\pi}{2} + \sin^{-1} \left[\frac{R (Y + R_n) - R_n (2Y + R_n)}{RY} \right]}{\frac{\pi}{2} + \sin^{-1} \left[\frac{R_t (Y + R_n) - R_n (2Y + R_n)}{R_t Y} \right]} \tag{57}$$

Equation (57) determines R (or R^*) as a function of L^*. The quantity L^* varies from 0 at the n-boundary (fig. 13(a)) to 1.0 at the t-boundary, as does the coordinate M. Equations (56) and (57) determine α as a function of L^*. The quantities R^* and α are tabulated as functions of L^* in table II.

Lines of constant L^* and θ^* on the surface of revolution and on the flat transformed plane are shown in figures 13(a) and 13(b), respectively. The equations in this report were developed for surfaces of revolution (dM and $d\theta$ coordinates), but, if dM is replaced by $R(\Delta L)\ dL^*$, the equations also apply to the flat transformed surfaces.

Prescribed conditions. - In addition to the surface of revolution which has already been described, the following conditions are prescribed:

$$H^* = 15-14R^*$$

$$U_T = 1.5$$

$$\lambda_U = 0.2$$

$$\lambda_D = 2.0$$

and

$$\varphi = 1.05$$

These prescribed conditions were selected to result in (approximately):

$$(Q_{av})_n = 0.50$$

$$\beta_n = -45^\circ$$

$$\delta_n = 0.85$$

$$(Q_{av})_t = 0.90$$

$$\delta_t = 0.95$$

Prescribed velocity distribution. - The prescribed velocity distribution for the second numerical example was obtained from equations (50a) and (50b) with x instead of M as the independent variable, where

$$x = 2R^* - 1 \tag{58}$$

The prescribed conditions on the velocity distribution are:

$$(Q_{av})_n = 0.5$$

$$(Q_{av})_t = 0.9$$

$$\left.\left(\frac{dQ_{av}}{dx}\right)_n = 0.35\right\} \text{ chosen so that } \left(\frac{dQ_0}{dx}\right)_n = -0.5$$

$$\left.\left(\frac{dQ_{av}}{dx}\right)_t = 0.55\right\} \text{ chosen so that } \left(\frac{dQ_1}{dx}\right)_t = 0$$

$$(\Delta Q)_n = 0.1$$

$$(\Delta Q)_t = 0.2$$

$$(\Delta Q)_m = 0.5$$

$$x_m = 0.5$$

so that, from equations (50a), (50b), (51), and (52),

$$Q_{av} = 0.50 + 0.35x - 0.05x^2 + 0.10x^3$$

$$\Delta Q = 0.10 + 1.70x - 2.00x^2 + 0.40x^3$$

from which Q_0 and Q_1 are obtained by equations (49a) and (49b).

The resulting velocity distribution as a function of L^* is given in table II and is plotted in figure 14. As a result of this velocity distribution the solidity σ is equal to 2.561 (from equation (21)), and the number of blades b is 12 (from equation (53)). In order to obtain this even number of blades, the downstream whirl λ_D was adjusted (as indicated by equation (21)) from the prescribed value of 2.000 to 1.939. The pressure difference ΔP and the average relative tangential velocity $(Q_\theta)_{av}$ are tabulated as functions of L^* in table II.

Results. - The values of β, δ, and R^* that determine the blade-element profile for the first approximation are given as functions of L^* in table II together with the values of $\beta_{0.5}$, δ, $X_{0.5}$, and R^* that determine the blade-element profile for the second approximation. The blade-element profile obtained by the second approximation is plotted on the surface of revolution in figure 13(a) and on the flat transformed $L^*\theta^*$-plane in figure 13(b). (The nose and tail of the blade-element are rounded off in an arbitrary manner.) The blades are curved forward in the direction of rotation at the impeller tip, because the prescribed value of λ_D is greater than U_T.

The variation in thickness of the blade-element profile at values of L^* toward the impeller tip is considered rapid because, for the relatively large values of β that exist at these values of L^*, the difference $(\tan \beta_1 - \tan \beta_0)$ is large, which condition makes inaccurate the assumption that $\Delta\beta$ is constant circumferentially across the channel between blade elements (see section on flow direction $\beta_{0.5}$). The rapid variation in thickness can and should be eliminated by different prescribed variations in H^* and Q_{av} or both with L^*.

The streamlines and their normals, used by the stream-filament method to estimate velocities along the blade-element surfaces, are plotted on the $L^*\theta^*$-plane in figure 13(b).

The velocities obtained by the stream-filament method on the $L^*\theta^*$-plane are compared in figure 14 with the prescribed velocities as a function of L^*. The comparison is excellent, except at large values of L^* where the rapid variation in blade-element-profile thickness and the small radii of curvature along the blade-element profile at the tip (fig. 13(a)) violate assumptions of the design method. Thus the design method is limited to prescribed velocities that result in blade-element profiles with gradual variations in thickness and with minimum radii of curvature at least approximately equal to the channel width between profiles.

The resulting blade-element profiles for the first and second approximations are compared in figure 15. The two profiles are quite similar, except near the tail (where neither approximation is satisfactory because of the rapid variation in blade-element-profile thickness and the small radii of curvature at the blade-element tip). Although the difference in profiles is small, the difference may be significant because of the small blade spacing. However, at least for rough calculations, the first approximation appears to be satisfactory for centrifugal impellers with blade-element solidities as high as that of the second numerical example $(\sigma \approx 2.5)$.

SUMMARY OF RESULTS AND CONCLUSIONS

An approximate blade-element-design method is developed for compressible or incompressible nonviscous flow in high-solidity stators or rotors of axial-, radial-, or mixed-flow compressors, turbines, or two-dimensional cascades. The method is based upon channel-type flow between blade elements on a specified surface of revolution that is concentric with the axis of the compressor or turbine. The blade element is designed for prescribed velocities along the blade-element profile as a function of the meridional distance. The blade-element-design method is developed in two parts, called the first and second approximations, either of which may be used to determine the blade-element profile. The first approximation, which is simple and rapid, assumes that circumferentially across the channel between blade elements the velocity is constant and the flow direction is equal to that of the blade-element camber line. The second approximation, which is more complex and less rapid, partially corrects for the variation in velocity and for the change in flow direction across the channel between blade elements.

Two numerical examples are presented. The first example is the design of a blade-element profile for a plane two-dimensional cascade in compressible flow with prescribed velocities along the profile. The second example is the design of a blade element for the impeller of a mixed-flow centrifugal compressor. As a result of these numerical examples, the following conclusions have been drawn:

1. The blade-element-design method is limited to prescribed velocities that result in blade-element profiles with gradual variations in thickness and with minimum radii of curvature at least approximately equal to the channel width between profiles. (The nose and tail regions of the blade-element profile are not considered by this blade-element-design method.)

2. For centrifugal impellers with blade-element solidities as high as that of the second numerical example (2.561), the first approximation appears to be satisfactory, at least for rough calculations.

3. The blade-element-design method is not recommended for solidities lower than that of the first example (1.215).

4. For blade-element solidities as low as that for the first example (1.215), the second approximation is required.

Lewis Flight Propulsion Laboratory,
National Advisory Committee for Aeronautics,
Cleveland, Ohio, March 26, 1951.

APPENDIX A

SYMBOLS

The following symbols are used in this report:

A	coefficient, defined by equation (C5)
a_o	characteristic velocity, absolute stagnation speed of sound upstream of blade-element row where conditions are uniform in circumferential direction
B	coefficient, defined by equation (C6)
b	number of blade elements (or passages between blade elements)
C	coefficient, defined by equation (C7)
c	characteristic length, blade chord measured from n-boundary to t-boundary along meridional line on surface of revolution
d	coefficient, defined by equation (51)
E	coefficient, defined by equation (C3a)
e	coefficient
exp	exponential, $\exp(y) = e^y$
F	coefficient, defined by equation (C3b)
$(\Delta f)_T$	total (blocked and unblocked) incremental annulus area normal to direction of Q_M at blade-element tip, defined by equation (20)
g	acceleration due to gravity
ΔH	incremental height of fluid particle or blade element, measured normal to surface of revolution (fig. 5), (dimensionless, expressed in units of characteristic length c)
H^*	height ratio of blade element or fluid particle on surface of revolution (fig. 5), $\Delta H/(\Delta H)_T$
I	integrand

I_{linear} value of I if variation in I with X is linear

I^* integrand ratio, defined by equation (B1a)

j coefficient, defined by equation (52)

k coefficient, defined by equation (37a)

L transformed coordinate, defined by equation (55a)

ΔL change in L from n-boundary to t-boundary, defined by equation (55b)

L^* $(L-L_n)$ divided by ΔL (so that L^* varies from 0 to 1.0 along meridional line between n-boundary and t-boundary), defined by equation (54a)

M coordinate distance along meridional line on surface of revolution (fig. 6, for example) (dimensionless, expressed in units of characteristic length c; varies from 0 at n-boundary to 1.0 at t-boundary)

N coordinate distance measured normal to M on flat plane of two-dimensional cascade (dimensionless, expressed in units of characteristic length c)

P static-pressure ratio, p/p_o, defined by equation (9)

ΔP change in P circumferentially across channel between blade elements, defined by equation (16)

p static (stream) pressure

Q relative velocity on surface of revolution (dimensionless, expressed in units of characteristic velocity a_o) (fig. 3)

ΔQ change in Q circumferentially across channel between blade elements, defined by equation (48)

R cylindrical coordinate (dimensionless, expressed in units of characteristic length c) (fig. 3)

R^* ratio, R/R_T

S distance along streamline on surface of revolution (dimensionless, expressed in units of characteristic length c) (fig. 3)

T	static (stream) temperature
U_T	tip speed of blade element, defined by equation (4)
Δw	total incremental flow rate along surface of revolution with incremental annulus height ΔH
X	ratio (circumferential distance from 0-streamline to point in channel divided by channel width in circumferential direction), defined by equation (30)
x	defined by equation (58)
Y	radius of meridional line on surface of revolution in second numerical example (dimensionless, expressed in units of characteristic length c) (fig. 12)
Z	cylindrical coordinate (dimensionless, expressed in units of characteristic length c) (fig. 3)
α	slope of surface of revolution, equation (1) (fig. 3)
β	direction on surface of revolution, equation (2) (fig. 3)
$\Delta\beta$	correction for direction β, defined by equation (39)
β'	uncorrected flow direction on surface of revolution, defined by equation (39)
γ	ratio of specific heats
δ	channel-width ratio (circumferential width of channel divided by circumferential spacing of blades), defined by equation (12)
δ'	uncorrected channel-width ratio (from first approximation or from previous cycle of second approximation)
θ	cylindrical coordinate (positive about Z-axis according to right-hand rule) (fig. 3)
$\Delta\theta$	angular spacing of blades about Z-axis, defined by equation (53)
θ^*	coordinate θ divided by ΔL, defined by equation (54b)
λ	whirl ratio, defined by equation (8)

ξ integrand ratio, defined by equation (B1b)

ρ static (stream) density

σ blade-element solidity, defined by equation (11)

φ flow coefficient, defined by equation (19)

ψ stream function, defined by equation (36)

ω angular velocity of rotor (in direction of positive θ)

Subscripts:

a,b,c,d successive points

av mass-weighted average value across channel in θ-direction between blade elements

D boundary downstream of blade elements where conditions are uniform in θ-direction

M component along meridional line on surface of revolution

m quantities associated with maximum value of ΔQ

n n-boundary near nose of blade-element profile (fig. 6, for example)

o absolute stagnation condition upstream of blade-element row where conditions are uniform in circumferential direction

R,θ,Z components in positive R-, θ-, and Z-directions, respectively

T tip (maximum radius) of blade element

t t-boundary near tail of blade-element profile (fig. 6, for example)

U boundary upstream of blade elements where conditions are uniform in circumferential direction

0 left channel wall, when viewed in direction of Q_M (fig. 8)

0.5 0.5-streamline that equally divides flow between blade elements (fig. 8)

$\frac{1}{2}$ value at X equals 0.5

1 right channel wall, when viewed in direction of Q_M (fig. 8)

APPENDIX B

VARIATION IN $X_{0.5}$ FOR VARIOUS PARABOLIC DISTRIBUTIONS OF INTEGRAND $\left(\frac{\rho}{\rho_o} Q \cos \beta'\right)$ IN X-DIRECTION

The ratio $X_{0.5}$ is defined by equation (36a). This ratio determines the position of the mean (0.5-) streamline, which equally divides the flow between two blade elements. The ratio $X_{0.5}$ is therefore the value of X that equally divides the area under the curve of the integrand I (equal to $\frac{\rho}{\rho_o} Q \cos \beta'$) against X. If I is assumed to vary in a parabolic manner (see assumptions of second approximation) and if I has the values I_0 at X equals 0, $I_{\frac{1}{2}}$ at X equals 0.5, and I_1 at X equals 1.0, then

$$I^* = \left(\frac{2}{1+\xi}\right) + 2\left(2\, I^*_{\frac{1}{2}} - \frac{3+\xi}{1+\xi}\right) X + 4\left(1 - I^*_{\frac{1}{2}}\right) X^2 \quad . \tag{B1}$$

where

$$I^* = \frac{I}{(I_{linear})_{\frac{1}{2}}} \tag{B1a}$$

$$\xi = \frac{I^*_1}{I^*_0} \tag{B1b}$$

in which

$$(I_{linear})_{\frac{1}{2}} = \frac{1}{2}\ (I_0 + I_1) \tag{B1c}$$

The integrand I^* in equation (B1) is dimensionless, having been divided by $(I_{linear})_{\frac{1}{2}}$, which from equation (B1c) is equal to the value of I at X equals 1/2 if the variation in I with X is linear. It was convenient to divide I by $(I_{linear})_{\frac{1}{2}}$ in order to facilitate the comparison of $X_{0.5}$ for linear and parabolic variations in I with X. The constant $I^*_{\frac{1}{2}}$ contained in equation (B1) is the ratio at X equal to 0.5 of the integrand $I_{\frac{1}{2}}$ for a parabolic variation in I

to the integrand $(I_{linear})_{\frac{1}{2}}$ for a linear variation in I. Thus, $I^*_{\frac{1}{2}}$ is a direct measure of the deviation of the parabolic variation in I from a linear variation between the same values of I_0 and I_1. The ratio ξ (equation (B1b)) is a direct measure of the relative magnitudes of the integrand at X equals 0 and 1.0.

Substitution of equation (B1) into equation (36a) results in (after integration)

$$8\left(1-I^*_{\frac{1}{2}}\right)X^3_{0.5} + 6\left(2\,I^*_{\frac{1}{2}} - \frac{3+\xi}{1+\xi}\right)X^2_{0.5} + \left(\frac{12}{1+\xi}\right)X_{0.5}$$
$$= 4\left(1-I^*_{\frac{1}{2}}\right) + 3\left(2\,I^*_{\frac{1}{2}} - \frac{3+\xi}{1+\xi}\right) + \left(\frac{6}{1+\xi}\right) \tag{B2}$$

Equation (B2) gives $X_{0.5}$ as a function of the parameters $I^*_{\frac{1}{2}}$ and ξ. The equation has been solved for a wide range of $I^*_{\frac{1}{2}}$ and ξ, and the results are plotted in figure 16.

For infinite, blade-element solidity, $I^*_{\frac{1}{2}}$ and ξ become 1.0 so that (from fig. 16) $X_{0.5}$ becomes 0.5 (the value assumed, in effect, for the first approximation). As the solidity decreases from infinity, $I^*_{\frac{1}{2}}$ and ξ become different from 1.0 and $X_{0.5}$ becomes different from 0.5. In the second approximation of the blade-element-design method, the value ξ can be estimated but the value of $I^*_{\frac{1}{2}}$ cannot be determined conveniently. However, figure 16 shows that for all values of ξ (but especially for values of ξ between 1/2 and 2) the value of $X_{0.5}$ given by $I^*_{\frac{1}{2}}$ equal to 1.0 (that is, assuming a linear variation in I with X) is sufficiently accurate for the approximate methods of this report, provided $I^*_{\frac{1}{2}}$ lies between 0.8 and 1.2 (that is, provided the integrand deviates only moderately from a linear variation, as assumed in the second approximation, for high-solidity blade elements). And in any event, the values of $X_{0.5}$ so determined are more accurate than the value of 0.5 assumed by the first approximation.

For the two numerical examples of the design method in this report, $0.98 < I^*_{\frac{1}{2}} < 1.12$ and $0.8 < \xi < 2.1$. These ranges in $I^*_{\frac{1}{2}}$ and ξ resulted in values of $X_{0.5}$ between 0.47 and 0.59. Such a range of $X_{0.5}$ is typical of high-solidity blade-element profiles with minimum radii of curvature at least approximately equal to the channel width between profiles. (In reference 13, for example, the values of $X_{0.5}$ vary

between 0.50 and 0.58.) Therefore, for high-solidity blade-element profiles with relatively large radii of curvature that result in integrands $\left(\frac{\rho}{\rho_o} Q \cos \beta'\right)$ that deviate only moderately from linear variations in the X-direction, the value of $X_{0.5}$ depends more on the magnitude of the integrand at X equals 0 and 1.0 (measured by ξ, fig. 16), than on the magnitude of the deviation (measured by $I^*_{\frac{1}{2}}$, fig. 16). Thus, the value of $X_{0.5}$ determined by assuming a linear variation in I $\left(\text{that is, } \frac{\rho}{\rho_o} Q \cos \beta'\right)$ with X is sufficiently accurate for the purposes of this report.

APPENDIX C

VELOCITY DISTRIBUTION IN CIRCUMFERENTIAL DIRECTION ACROSS CHANNEL BETWEEN BLADE ELEMENTS

The variation in the relative velocity Q in the circumferential direction across the channel between high-solidity blade elements is determined from considerations of the absolute irrotational motion of the fluid. Consider a fluid particle on a surface of revolution (fig. 5). In the absence of entropy gradients the absolute motion of the fluid particle is irrotational so that

$$0 = \frac{\partial}{\partial M}\left[\left(R^* U_T + Q_\theta\right) R\right] - \frac{\partial}{\partial \theta}\left[Q_M\right]$$

which, from equations (11), (12), and (30), becomes

$$0 = \frac{2R^* U_T \sin\alpha}{R_T} + \frac{Q_\theta \sin\alpha}{R_T} + R^* \frac{\partial Q_\theta}{\partial M} - \frac{\sigma}{\delta'}\frac{\partial Q_M}{\partial X}$$

or, from equations (6a) and (6c), and with the assumption that for high-solidity blade elements the variation in β' across the channel is small and that this variation can be neglected in the differential equation so that $\beta' \approx \beta'_{0.5}$ is a function of M only,

$$0 = \frac{2R^* U_T \sin\alpha}{R_T} + \frac{Q \sin\beta'_{0.5} \sin\alpha}{R_T} + R^* Q \cos\beta'_{0.5} \frac{d\beta'_{0.5}}{dM} +$$

$$R^* \sin\beta'_{0.5} \frac{\partial Q}{\partial M} - \frac{\sigma \cos\beta'_{0.5}}{\delta'} \frac{\partial Q}{\partial X} \tag{C1}$$

Along the streamline,

$$\frac{dQ}{dM} = \frac{\partial Q}{\partial M} + \frac{\partial Q}{\partial \theta}\frac{d\theta}{dM} = \frac{\partial Q}{\partial M} + \frac{\partial Q}{\partial X}\frac{dX}{d\theta}\frac{d\theta}{dM}$$

and from equations (2a), (2b), (11), (12), and (30),

$$\frac{\partial Q}{\partial M} = \frac{dQ}{dM} - \frac{\sigma \tan\beta'_{0.5}}{\delta' R^*}\frac{\partial Q}{\partial X} \tag{C2}$$

The derivative dQ/dM varies in the X-direction across the channel between blade elements. The values dQ_0/dM and dQ_1/dM at X equals 0 and 1.0, respectively, are known from the prescribed variations in Q_0 and Q_1 with M. For high-solidity blade elements, it is assumed that the variation in dQ/dM with X can be approximated by a straight line so that

$$\frac{dQ}{dM} = E + F\,X \tag{C3}$$

where

$$E = \frac{dQ_0}{dM} \tag{C3a}$$

$$F = \frac{dQ_1}{dM} - \frac{dQ_0}{dM} \tag{C3b}$$

The differential equation (C1) when combined with equations (C2) and (C3) becomes

$$\frac{\partial Q}{\partial X} - AQ - B(E+FX) - C = 0 \tag{C4}$$

where

$$A = \frac{\delta'}{\sigma} \cos \beta'_{0.5} \left(\sin \beta'_{0.5} \frac{\sin \alpha}{R_T} + R^* \cos \beta'_{0.5} \frac{d\beta'_{0.5}}{dM}\right) \tag{C5}$$

$$B = \frac{\delta'}{\sigma} R^* \cos \beta'_{0.5} \sin \beta'_{0.5} \tag{C6}$$

$$C = 2\,\frac{\delta'}{\sigma} R^* U_T \cos \beta'_{0.5} \frac{\sin \alpha}{R_T} \tag{C7}$$

Equation (C4) can be integrated in the X-direction to give

$$Q = \left[Q_0 + \frac{B}{A}\left(E + \frac{F}{A}\right) + \frac{C}{A}\right] \exp\,(AX) - \frac{B}{A}\left(E + \frac{F}{A} + FX\right) - \frac{C}{A} \tag{C8}$$

where the constant of integration has been determined so that Q equals Q_0 at X equals 0. The distribution of Q circumferentially across the channel between blade elements is given by

equation (C8). The coefficients B, C, E, and F are given by equations (C6), (C7), (C3a), and (C3b), respectively. The coefficient A is selected so that Q is equal to Q_1 when X = 1.0. Thus from equation (C8),

$$B = -\frac{\left[Q_1 - Q_0 \exp(A)\right] + C\left[\frac{1 - \exp(A)}{A}\right]}{\left(E + \frac{F}{A}\right)\left[\frac{1 - \exp(A)}{A}\right] + \frac{F}{A}} \tag{C9}$$

which is solved by trial and error to obtain the proper values of A, that is, the value of A that satisfies the known value of B.

For small values of A, equations (C8) and (C9) become

$$Q = Q_0 \exp(AX) + BEX + C + (BEA + BF + CA)\left(\frac{X^2}{2!} + \frac{AX^3}{3!} + \frac{A^2X^4}{4!} + \ldots\right) \tag{C8a}$$

and

$$B = \frac{\left[Q_1 - Q_0 \exp(A)\right] - C - CA\left(\frac{1}{2!} + \frac{A}{3!} + \frac{A^2}{4!} + \ldots\right)}{E + (EA + F)\left(\frac{1}{2!} + \frac{A}{3!} + \frac{A^2}{4!} + \ldots\right)} \tag{C9a}$$

which forms for equations (C8) and (C9) eliminate "small differences of large numbers" that otherwise appear in the numerical calculations when A is small ($|A| < 0.2$).

APPENDIX D

CONSTANT $\Delta\beta$ IN DIRECTION OF θ

It is proposed to show that $\Delta\beta$ is approximately constant in the direction of θ (that is, in the direction of X) if $(\tan\beta - \tan\beta_{0.5})$ is small in the direction of θ (a condition that is approached in high-solidity blades with gradual variations in blade-element-profile thickness) and if $\Delta\beta$ is small. Consider the magnitude of $\Delta\beta$ at some point (X,M) if, for the same value of M, the initial flow direction $\beta'_{0.5}$ at $X_{0.5}$ is changed an amount $\Delta\beta_{0.5}$ with $X_{0.5}$ and δ remaining unchanged throughout the flow field.

From equations (11), (12), and (30),

$$\theta - \theta_0 = X \frac{\delta}{R_T\sigma} \tag{D1a}$$

and in particular

$$\theta_{0.5} - \theta_0 = X_{0.5} \frac{\delta}{R_T\sigma} \tag{D1b}$$

From equations (D1a) and (D1b),

$$\theta - \theta_{0.5} = \frac{1}{R_T\sigma} (X\,\delta - X_{0.5}\,\delta)$$

which, after differentiating with respect to M and multiplying by R, becomes

$$\tan\beta - \tan\beta_{0.5} = \frac{R^*}{\sigma}\left(\frac{d(X\delta)}{dM} - \frac{d(X_{0.5}\,\delta)}{dM}\right) \tag{D2a}$$

Also, for the initial values of β' with the same values of X and δ,

$$\tan\beta' - \tan\beta'_{0.5} = \frac{R^*}{\sigma}\left(\frac{d(X\delta)}{dM} - \frac{d(X_{0.5}\,\delta)}{dM}\right) \tag{D2b}$$

Because X and δ remain the same, equation (D2b) is subtracted from equation (D2a) to give

$$\tan\beta - \tan\beta' = \tan\beta_{0.5} - \tan\beta'_{0.5} \tag{D3}$$

But from equation (39),

$$\beta' = \beta - \Delta\beta$$

so that equation (D3) becomes

$$\tan \beta - \tan (\beta - \Delta\beta) = \tan \beta_{0.5} - \tan (\beta_{0.5} - \Delta\beta_{0.5})$$

which for small values of $\Delta\beta_{0.5}$ becomes

$$\tan \beta - \frac{\tan \beta - \tan \Delta\beta}{1 + \tan \beta \tan \Delta\beta} \approx \tan \beta_{0.5} - \frac{\tan \beta_{0.5} - \Delta\beta_{0.5}}{1 + \Delta\beta_{0.5} \tan \beta_{0.5}} \tag{D4}$$

But

$$\tan \beta_{0.5} = \tan \beta - (\tan \beta - \tan \beta_{0.5})$$

and, neglecting powers and products of $(\tan \beta - \tan \beta_{0.5})$ and $\Delta\beta_{0.5}$, which are assumed small, equation (D4) becomes

$$\frac{\tan \beta - \tan \Delta\beta}{1 + \tan \beta \tan \Delta\beta} \approx \frac{\tan \beta - \Delta\beta_{0.5}}{1 + \Delta\beta_{0.5} \tan \beta}$$

from which

$$\tan \Delta\beta \approx \Delta\beta_{0.5}$$

or, because $\Delta\beta_{0.5}$ is small,

$$\Delta\beta \approx \Delta\beta_{0.5} \tag{D5}$$

REFERENCES

1. Lighthill, M. J.: A Mathematical Method of Cascade Design. R. & M. No. 2104, British A.R.C., June 1945.

2. Hansen, Arthur G., and Yohner, Peggy L.: A Numerical Procedure for Designing Cascade Blades with Prescribed Velocity Distribution in Incompressible Potential Flow. NACA TN 2101, 1950.

3. Goldstein, Arthur W., and Jerison, Meyer: Isolated and Cascade Airfoils with Prescribed Velocity Distribution. NACA Rep. 869, 1947. (Formerly NACA TN 1308.)

2159

4. Costello, George R.: Method of Designing Cascade Blades with Prescribed Velocity Distributions in Compressible Potential Flows. NACA Rep. 978, 1950. (Formerly NACA TN's 1913 and 1970.)

5. Alpert, Sumner: Design Method for Two-Dimensional Channels for Compressible Flow with Application to High-Solidity Cascades. NACA TN 1931, 1949.

6. Betz, A., and Flügge-Lotz, I.: Design of Centrifugal Impeller Blades. NACA TM 902, 1939.

7. Wu, Chung-Hua: A General Through-Flow Theory of Flow with Subsonic or Supersonic Velocity in Turbomachines of Arbitrary Hub and Casing Shapes. NACA TN 2302, 1951.

8. Reissner, H. J.: On a Design Theory of Blade Systems in Steady Compressible Flow. Proc. Seventh Int. Congress Appl. Mech., vol. 2, pt. 2, 1948, pp. 612-613.

9. Hamrick, Joseph T., Ginsburg, Ambrose, and Osborn, Walter M.: Method of Analysis for Compressible Flow through Mixed-Flow Centrifugal Impellers of Arbitrary Design. NACA TN 2165, 1950.

10. Ruden, P.: Investigation of Single Stage Axial Fans. NACA TM 1062, 1944.

11. Stanitz, John D.: Two-Dimensional Compressible Flow in Turbomachines with Conic Flow Surfaces. NACA Rep. 935, 1949. (Formerly NACA TN 1744.)

12. Stanitz, John D., and Ellis, Gaylord O.: Two-Dimensional Compressible Flow in Centrifugal Compressors with Straight Blades. NACA Rep. 954, 1950. (Formerly NACA TN 1932.)

13. Wu, Chung-Hua, and Brown, Curtis A.: Method of Analysis for Compressible Flow Past Arbitrary Turbomachine Blades on General Surface of Revolution. NACA TN 2407, 1951.

TABLE I - FIRST NUMERICAL EXAMPLE

[Plane, two-dimensional cascade: β_U, 0°; β_D, 60°; Q_D, 0.750; Q_U, 0.290; φ, 0.278; σ, 1.215]

M	Q_{av}	ΔQ	Q_0	Q_1	ΔP	$(Q_\theta)_{av}$	β	δ	$\beta_{0.5}$	δ	$X_{0.5}$
							First approximation		Second approximation		
0	0.348	0.200	0.248	0.448	-0.091	0	0	0.850	2.9	0.890	0.559
.1	.396	.279	.256	.535	-.141	.036	5.3	.765	7.2	.816	.580
.2	.448	.338	.279	.617	-.189	.088	11.3	.701	12.3	.751	.586
.3	.503	.378	.315	.692	-.230	.153	17.7	.661	17.7	.702	.581
.4	.559	.398	.360	.757	-.259	.230	24.3	.642	23.5	.673	.568
.5	.611	.398	.412	.810	-.275	.314	30.9	.644	29.6	.666	.549
.6	.659	.378	.470	.848	-.273	.400	37.3	.667	35.9	.680	.527
.7	.699	.338	.530	.868	-.252	.482	43.6	.711	42.1	.716	.506
.8	.730	.279	.590	.869	-.212	.555	49.5	.779	47.9	.769	.490
.9	.748	.199	.648	.847	-.154	.613	55.0	.874	52.8	.834	.480
1.0	.751	.100	.701	.801	-.078	.650	59.9	.996	56.4	.901	.474

NACA

TABLE II - SECOND NUMERICAL EXAMPLE

[Mixed-flow impeller for centrifugal compressor: λ_U, 0.2; λ_D, 1.939; φ, 1.05; σ, 2.561]

L^*	M	R^*	H^*	α	Q_{av}	ΔQ	Q_0	Q_1	ΔP	$(Q_\theta)_{av}$	β	δ	$\beta_{0.5}$	δ	$X_{0.5}$
											First approximation		Second approximation		
0	0	0.5	8.0	0	0.500	0.100	0.450	0.550	-0.060	-0.350	-44.4	0.853	-44.5	0.860	0.497
.1	.078	.503	7.955	3.5	.502	.111	.447	.558	-.067	-.289	-35.2	.739	-34.9	.741	.506
.2	.158	.513	7.817	7.1	.509	.143	.438	.581	-.089	-.230	-26.9	.661	-26.5	.664	.517
.3	.239	.530	7.580	10.8	.521	.195	.423	.618	-.125	-.159	-17.8	.596	-17.4	.603	.529
.4	.324	.555	7.231	14.6	.538	.263	.406	.670	-.178	-.065	-6.9	.542	-6.5	.555	.542
.5	.413	.589	6.753	18.6	.561	.342	.391	.732	-.247	.063	6.4	.507	6.8	.529	.553
.6	.509	.634	6.118	22.9	.592	.420	.382	.803	-.334	.226	22.4	.505	22.9	.537	.555
.70	.612	.694	5.290	27.6	.634	.482	.393	.875	-.433	.414	40.8	.573	41.6	.617	.541
.75	.668	.729	4.787	30.1	.660	.498	.411	.909	-.484	.501	49.4	.647	50.4	.698	.528
.800	.726	.770	4.215	32.7	.690	.498	.442	.939	-.531	.588	58.4	.788	59.6	.843	.510
.825	.757	.793	3.900	34.1	.708	.490	.463	.953	-.551	.622	61.5	.863	62.7	.910	.525
.850	.788	.817	3.563	35.5	.727	.476	.489	.965	-.566	.647	62.8	.906	63.8	.940	.547
.875	.821	.843	3.204	36.9	.749	.455	.521	.976	-.575	.658	61.5	.884	61.9	.921	.581
.900	.854	.870	2.819	38.4	.772	.425	.560	.985	-.574	.653	57.7	.815	56.5	.825	.570
.925	.889	.899	2.409	40.0	.799	.386	.606	.991	-.560	.631	52.2	.751	49.8	.745	.553
.950	.925	.931	1.971	41.6	.828	.336	.660	.996	-.526	.588	45.2	.719	41.0	.704	.520
.975	.962	.964	1.502	43.3	.862	.275	.725	.999	-.466	.523	37.4	.747	32.6	.744	.463
.9875	.981	.982	1.255	44.1	.880	.239	.760	1.000	-.423	.482	33.2	.800	29.8	.829	.430
1.0	1.0	1.0	1.0	45.0	.900	.200	.800	1.0	-.370	.439	29.2	.906	25.8	.958	.421

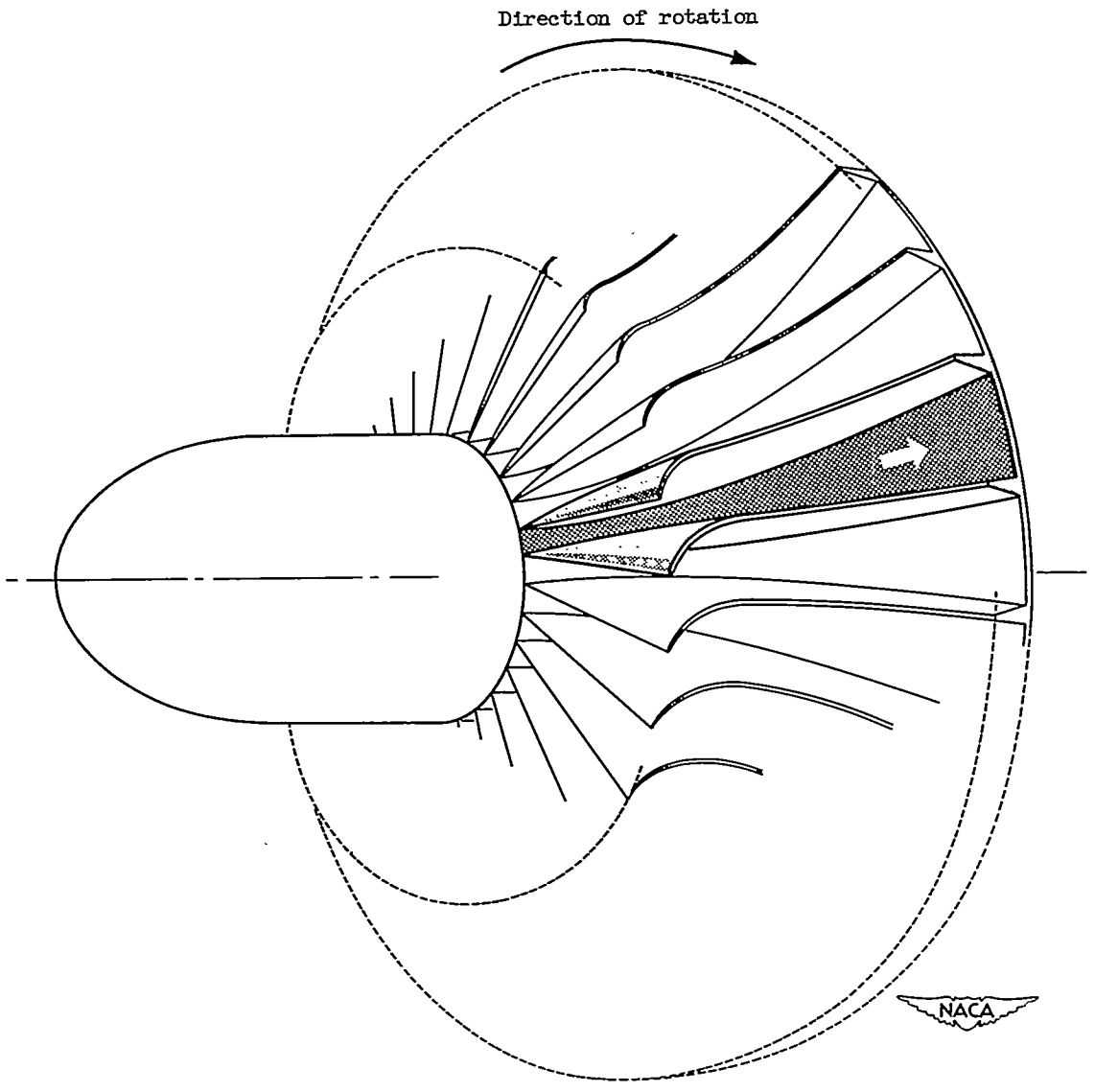

Figure 1. - Channel between blades of typical high-solidity blade row.

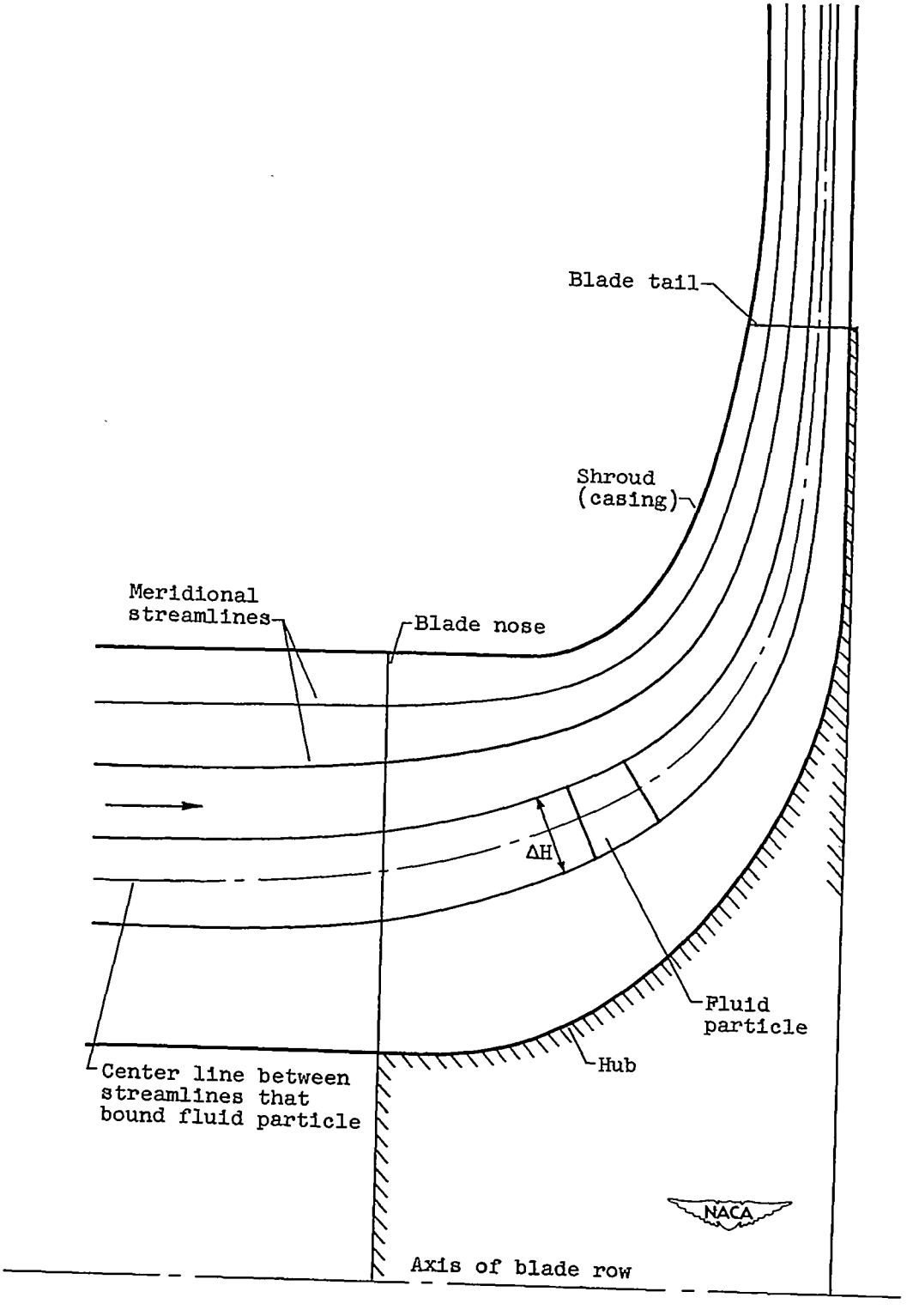

Figure 2. - Streamlines in meridional plane for axial-symmetry solution of flow through high-solidity blade row of figure 1.

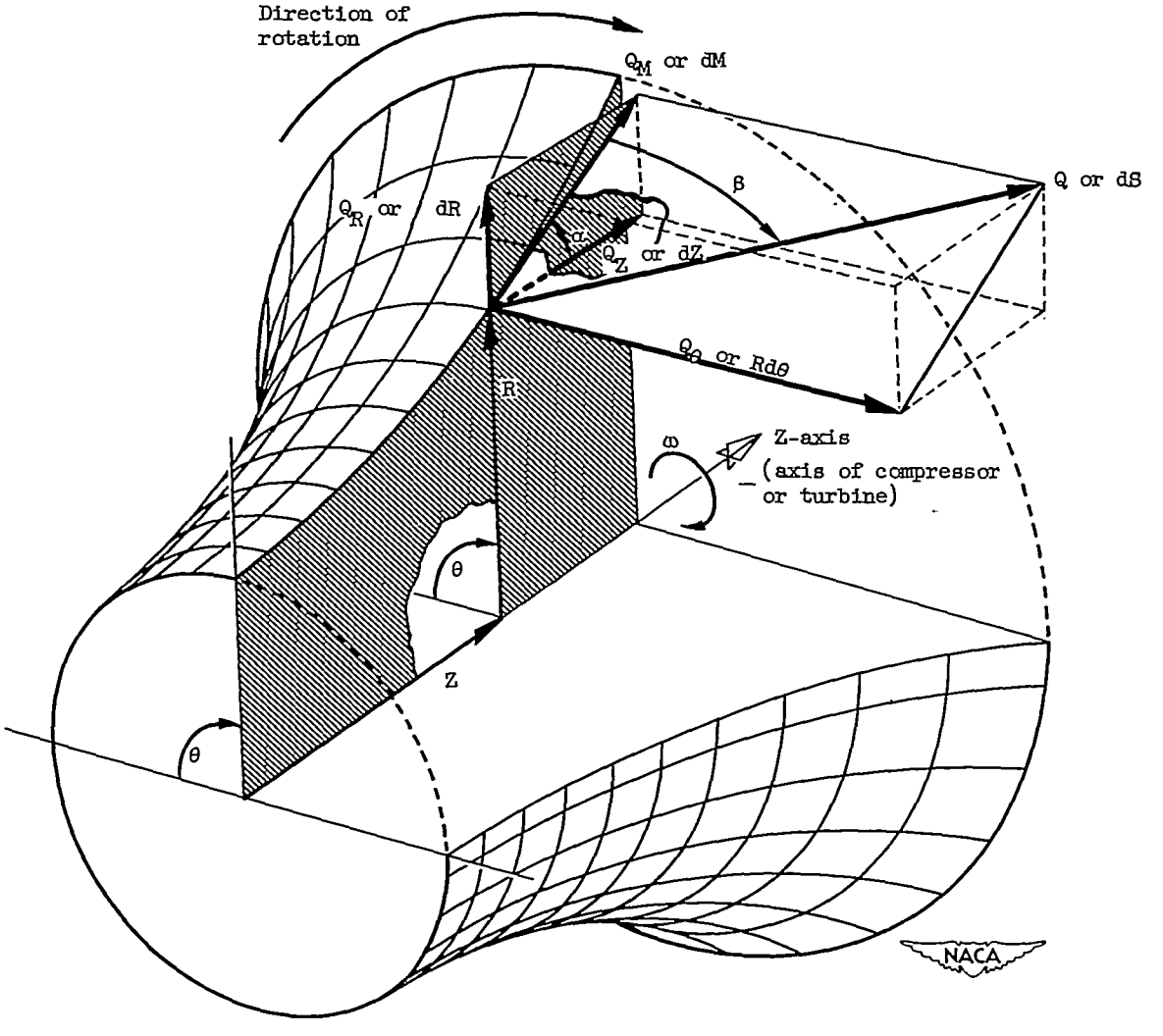

Figure 3. - Surface of revolution with coordinates and velocity components.

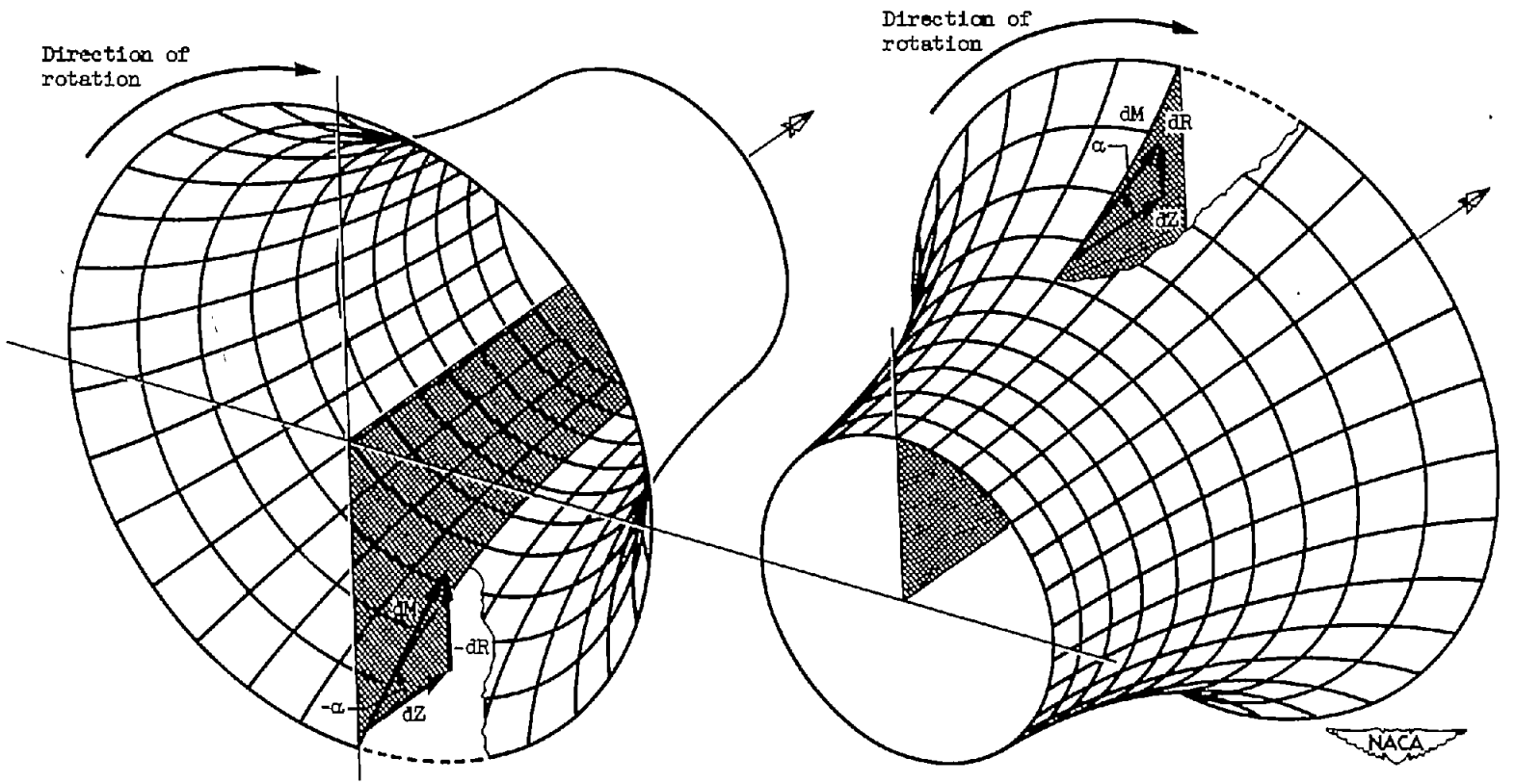

(a) Inflow machine.

(b) Outflow machine.

Figure 4. - Sign convention for typical inflow and outflow machines.

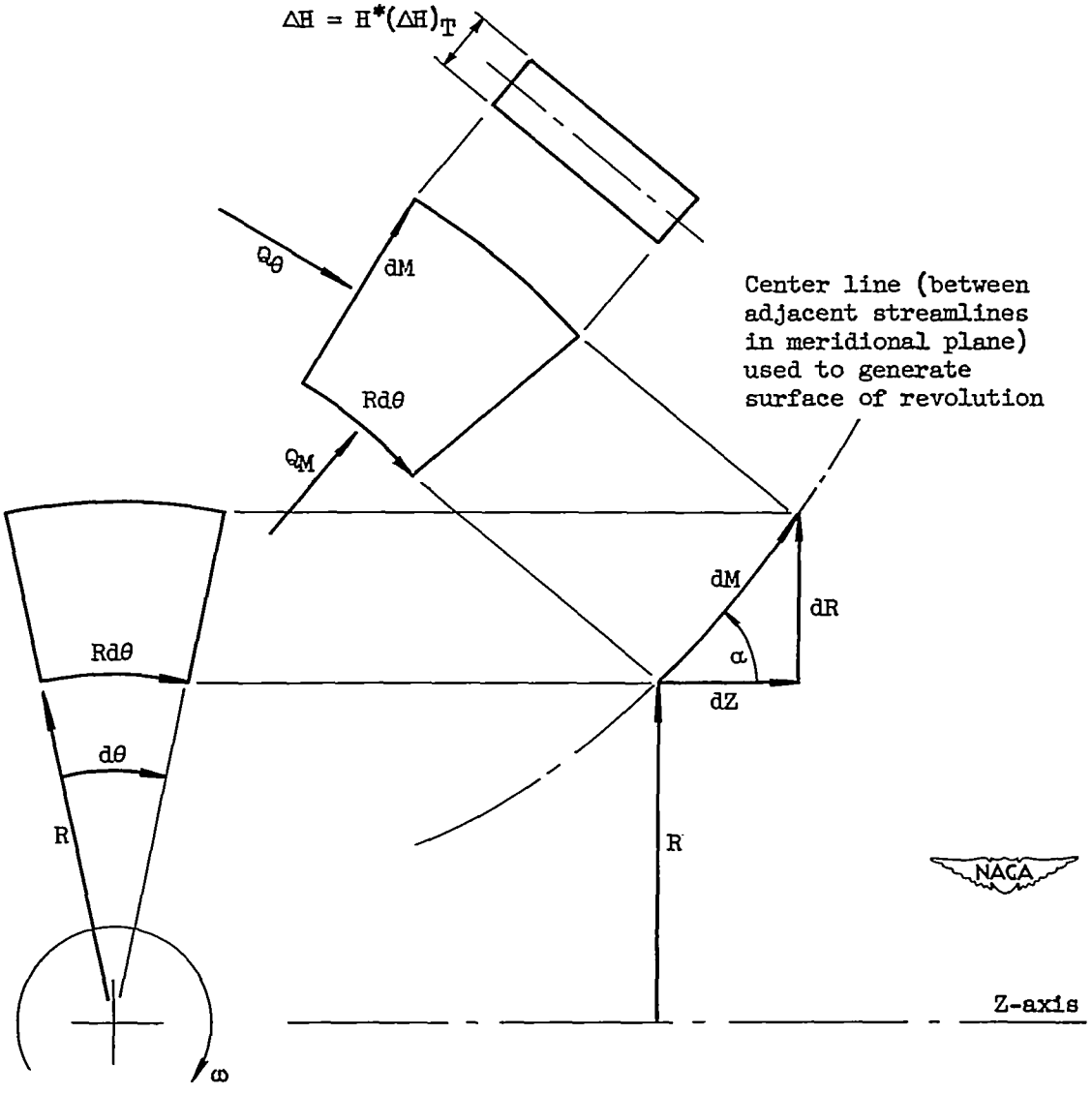

Figure 5. - Fluid particle on surface of revolution.

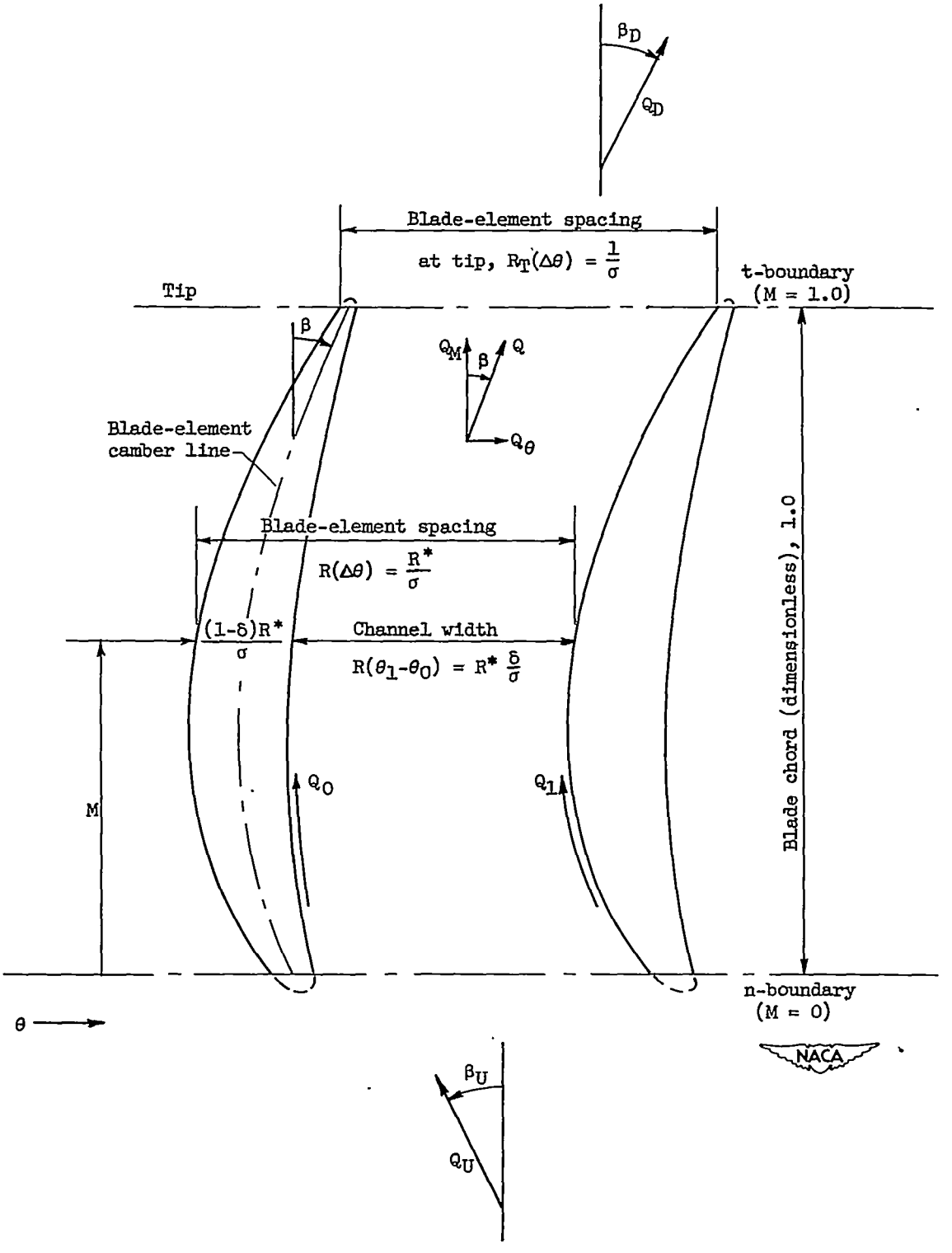

Figure 6. - View of passage between two blade-element profiles on θM-plane showing parameters used in first approximation.

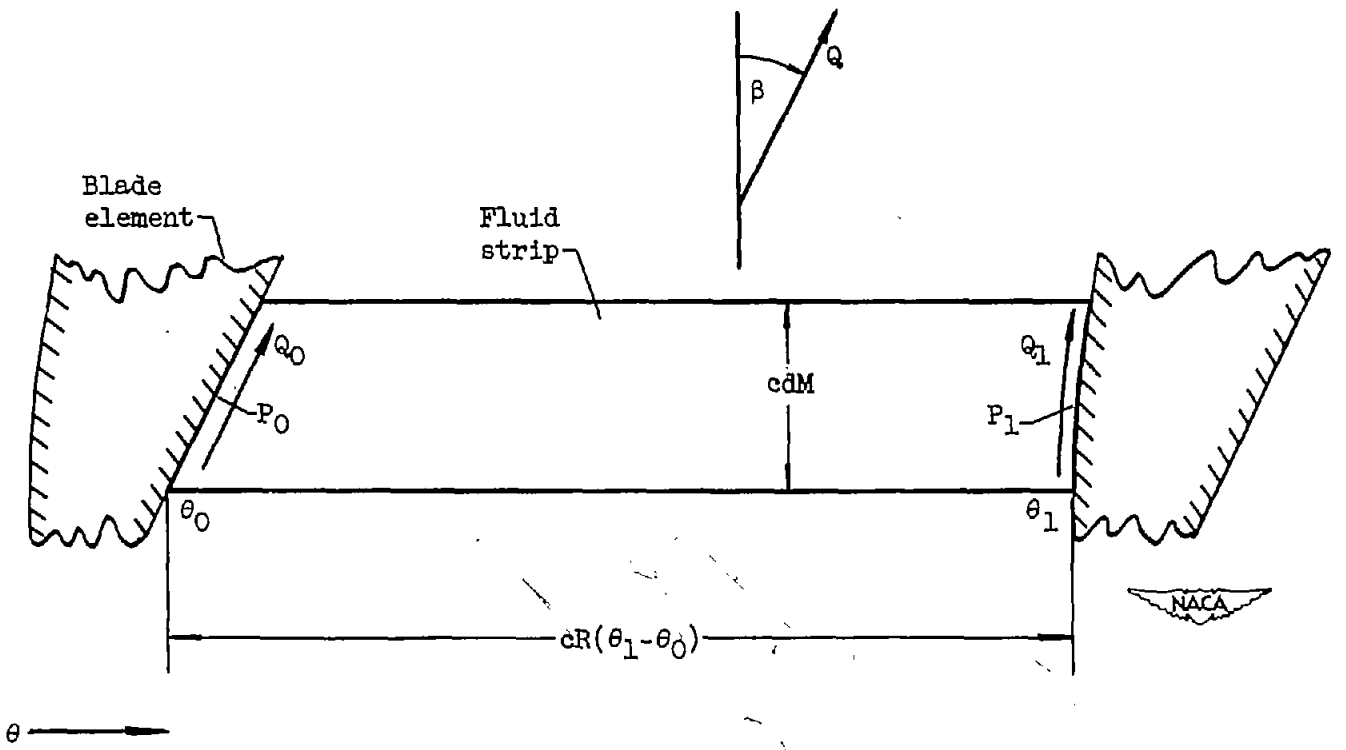

Figure 7. - Fluid strip between blade elements on surface of revolution.

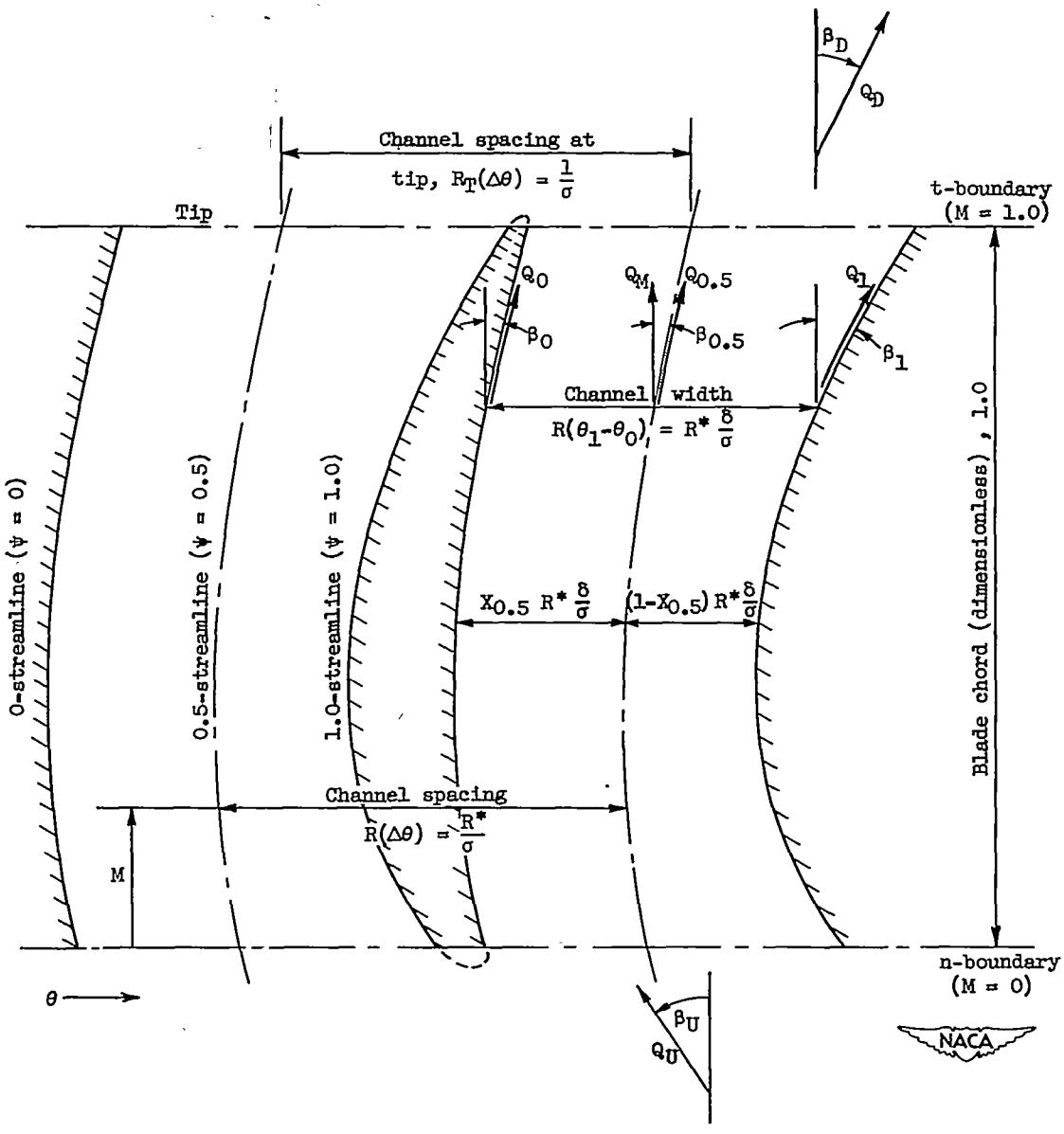

Figure 8. - View of passage between blade-element profiles on θM-plane showing parameters used in second approximation.

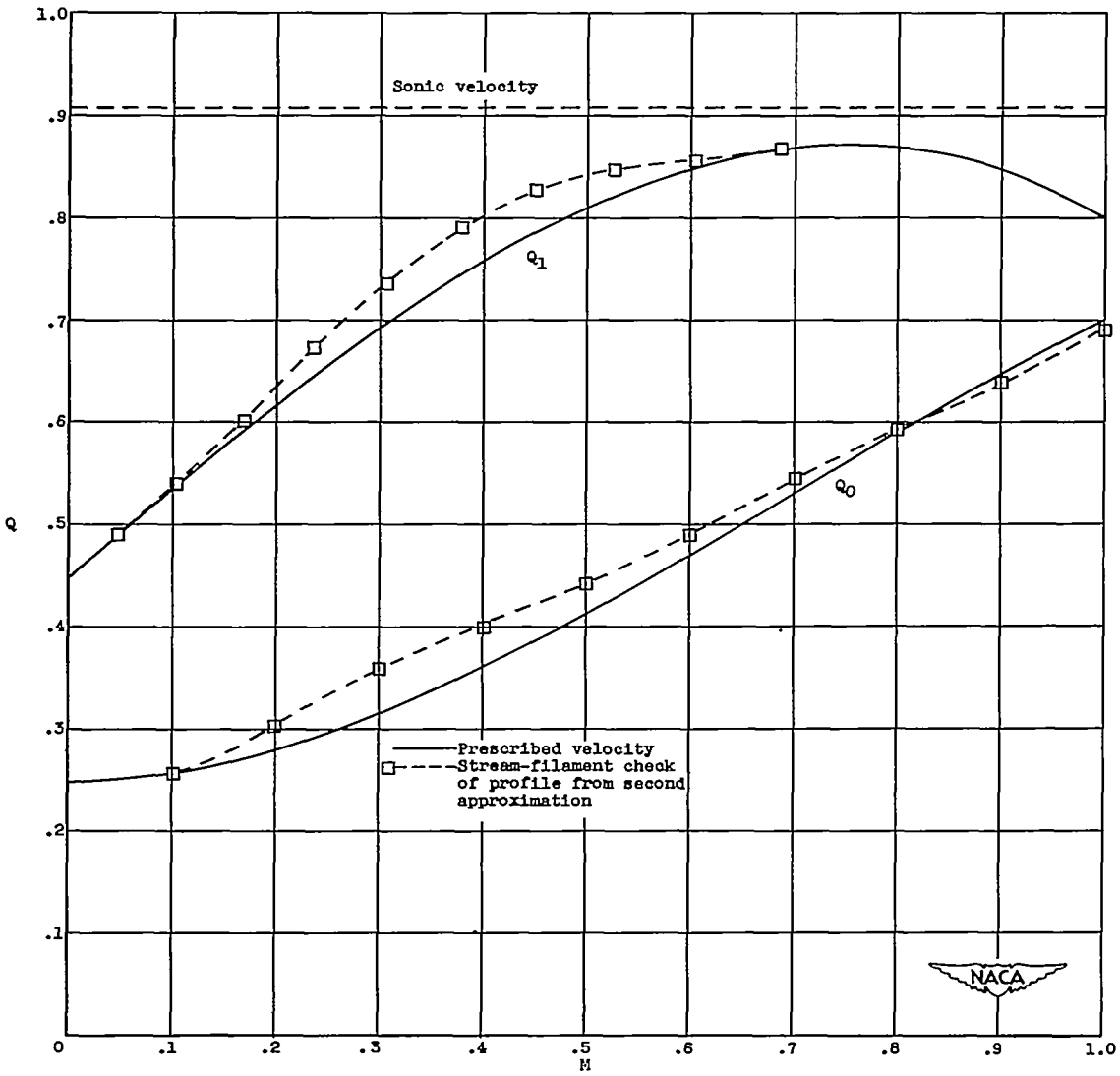

Figure 9. - Comparison of prescribed velocities for first numerical example with velocities obtained by stream-filament check of profile obtained by second approximation.

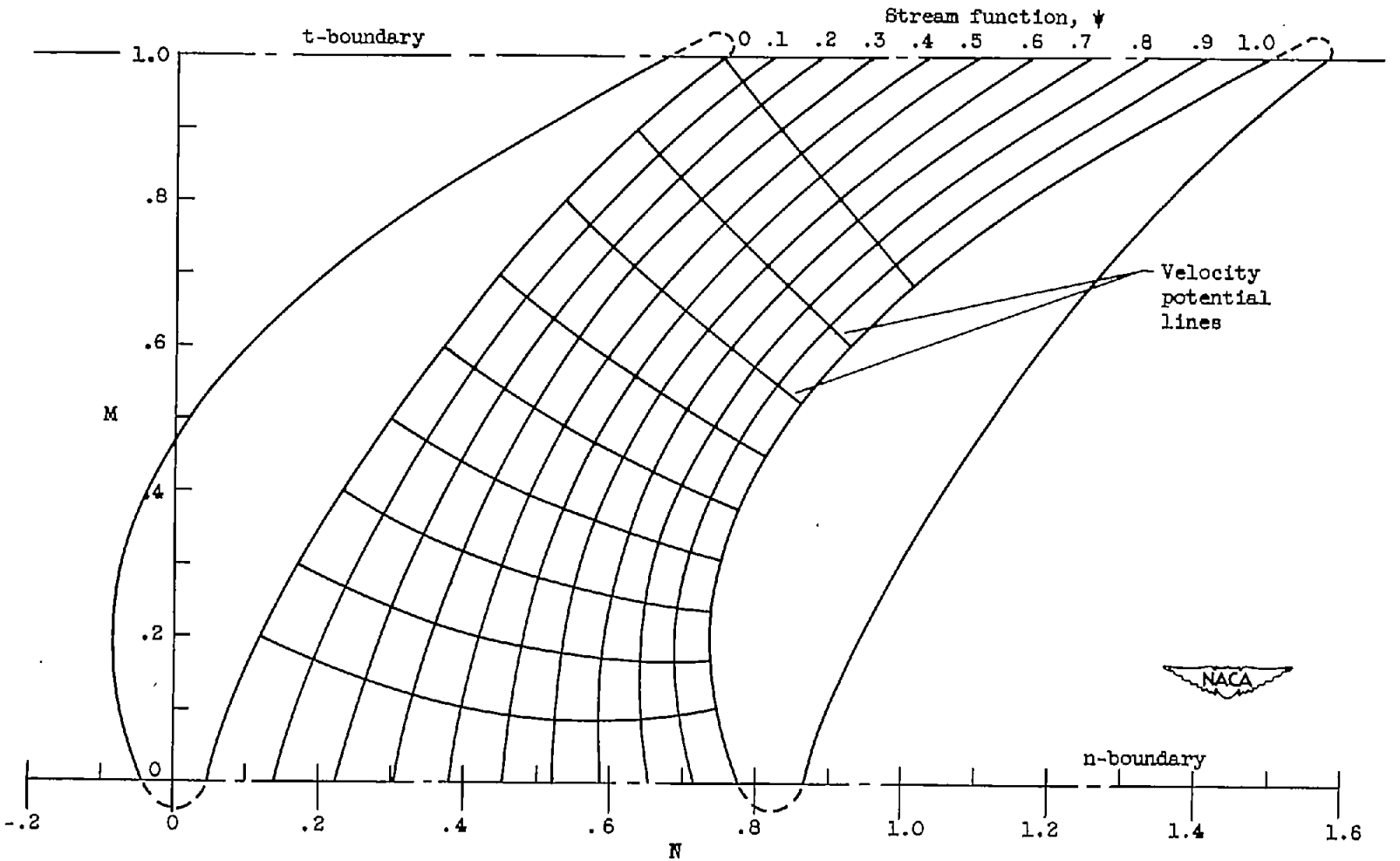

Figure 10. - Blade-element profile for first numerical example showing streamlines and velocity potential lines used in stream-filament check.

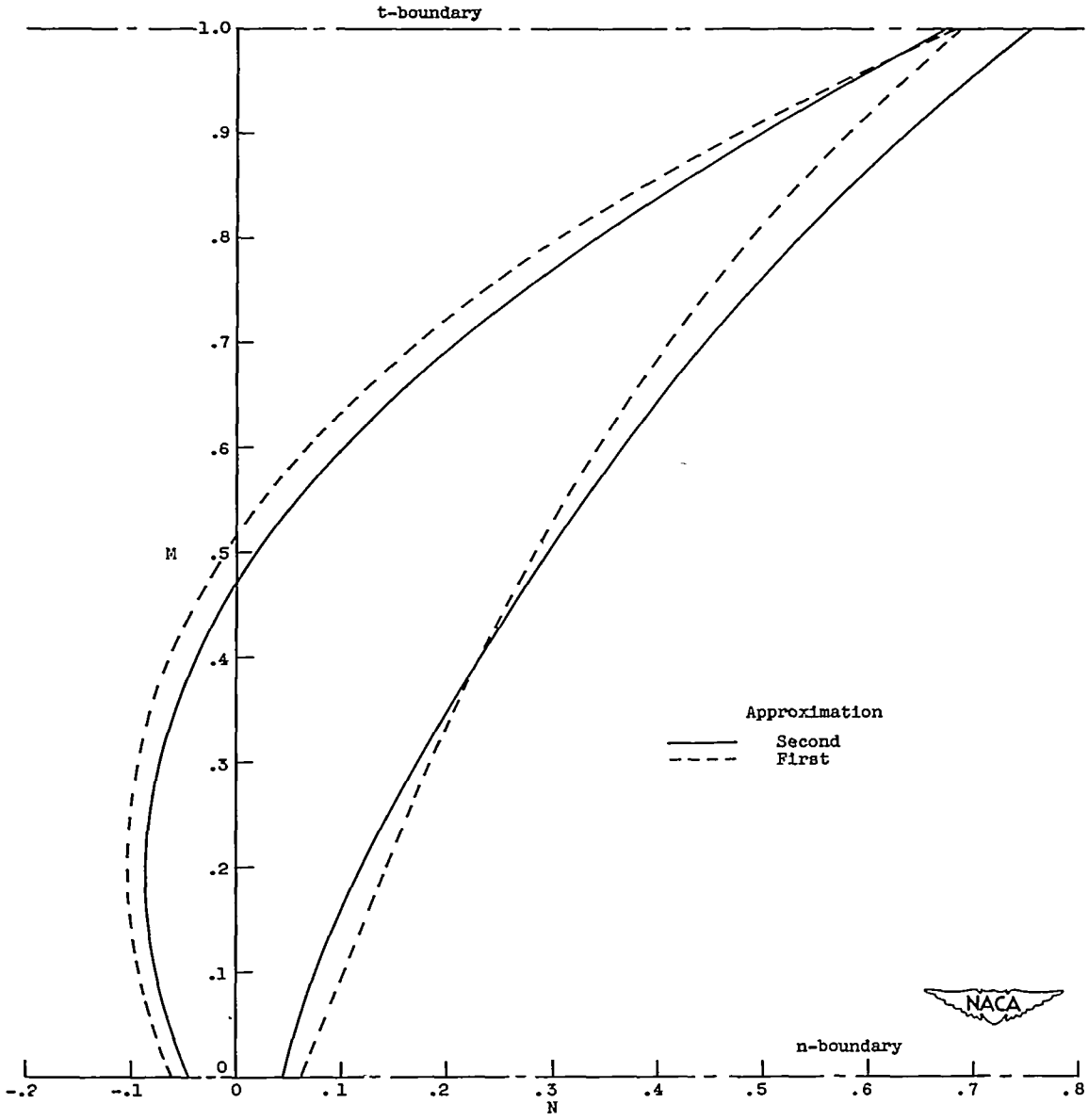

Figure 11. - Comparison of blade-element profiles obtained by first and second approximations for first numerical example.

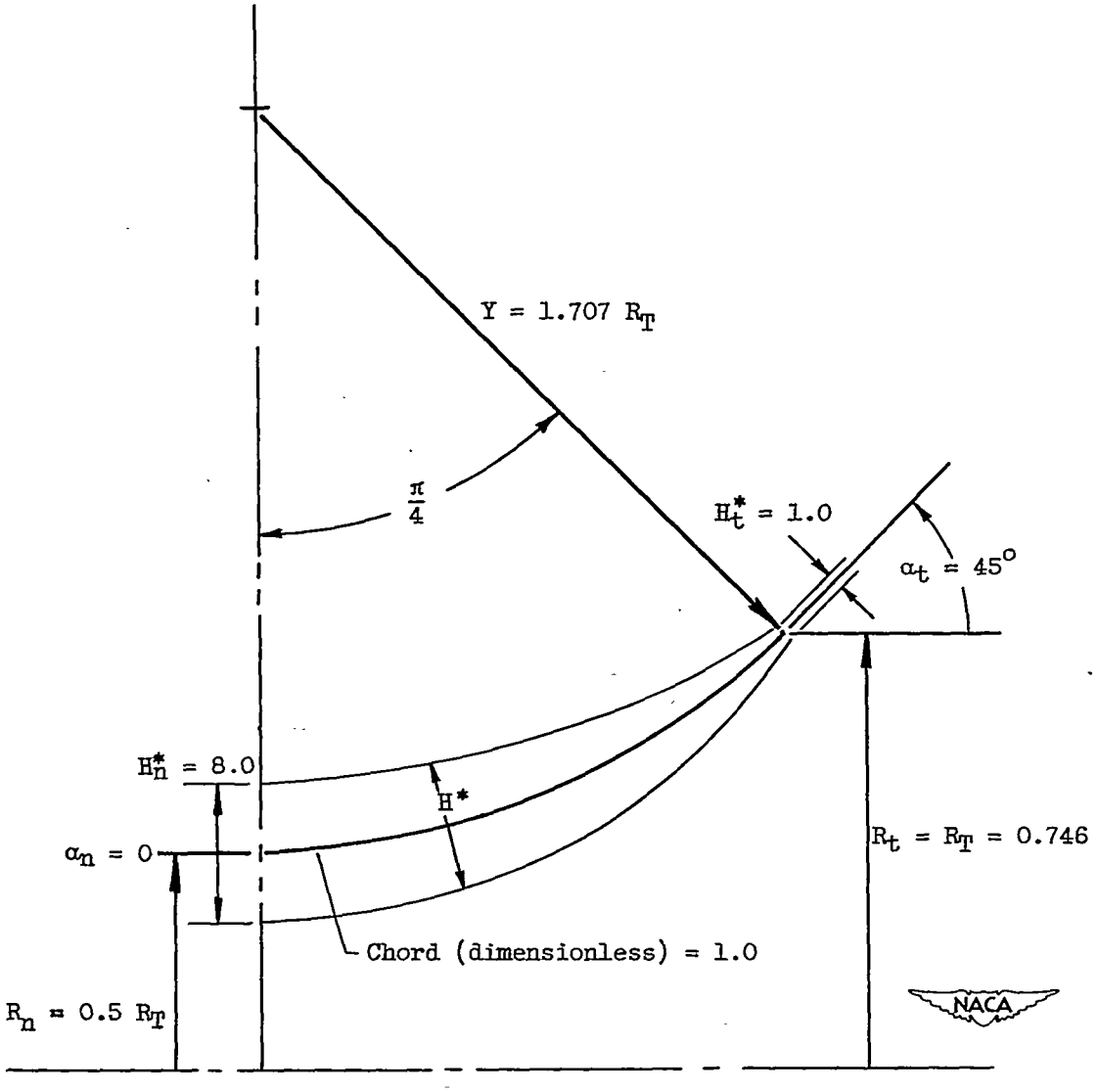

Figure 12. - Circular arc used to generate surface of revolution for second numerical example. Variation in H^* along circular arc also shown.

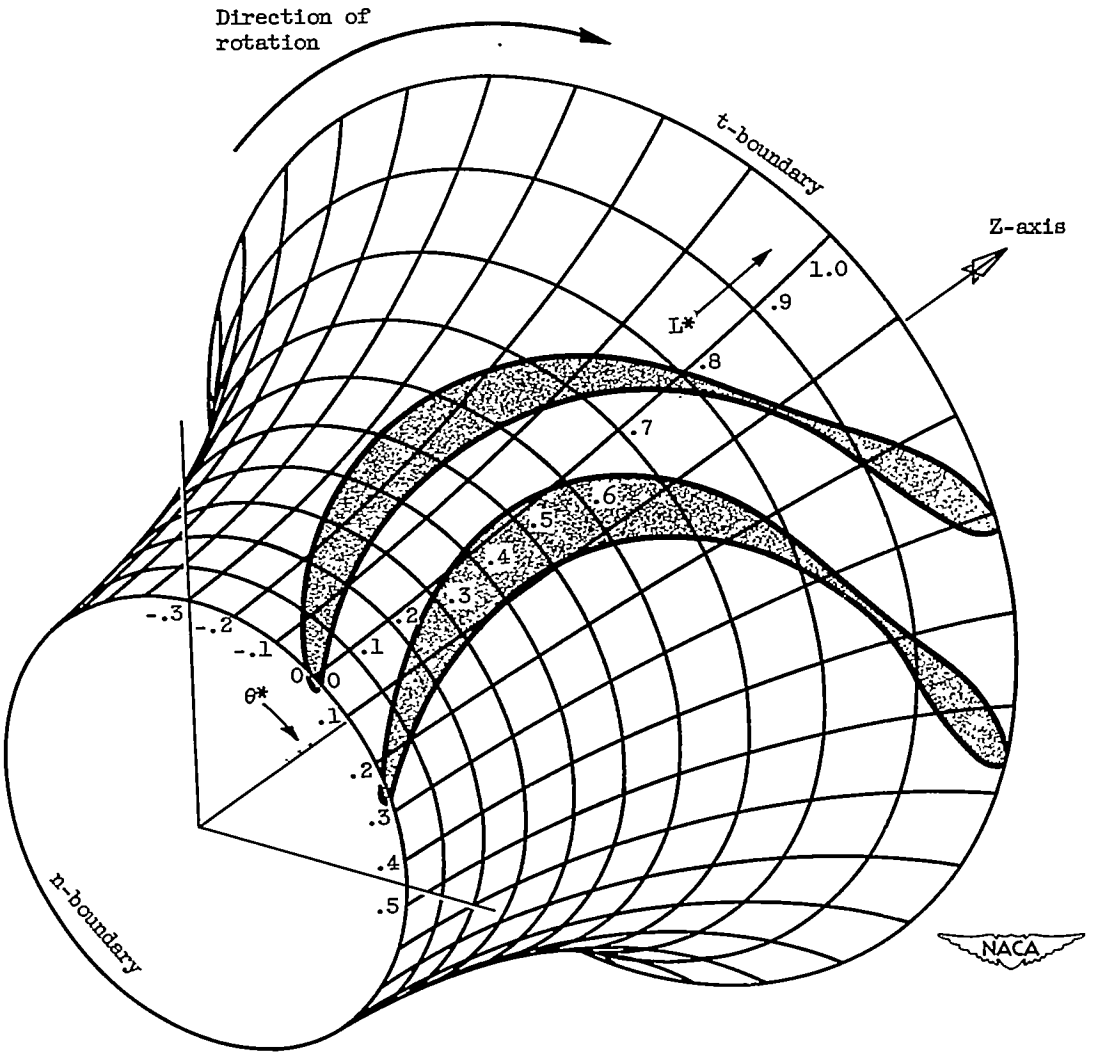

(a) Surface of revolution.

Figure 13. - Blade-element profile for second numerical example.

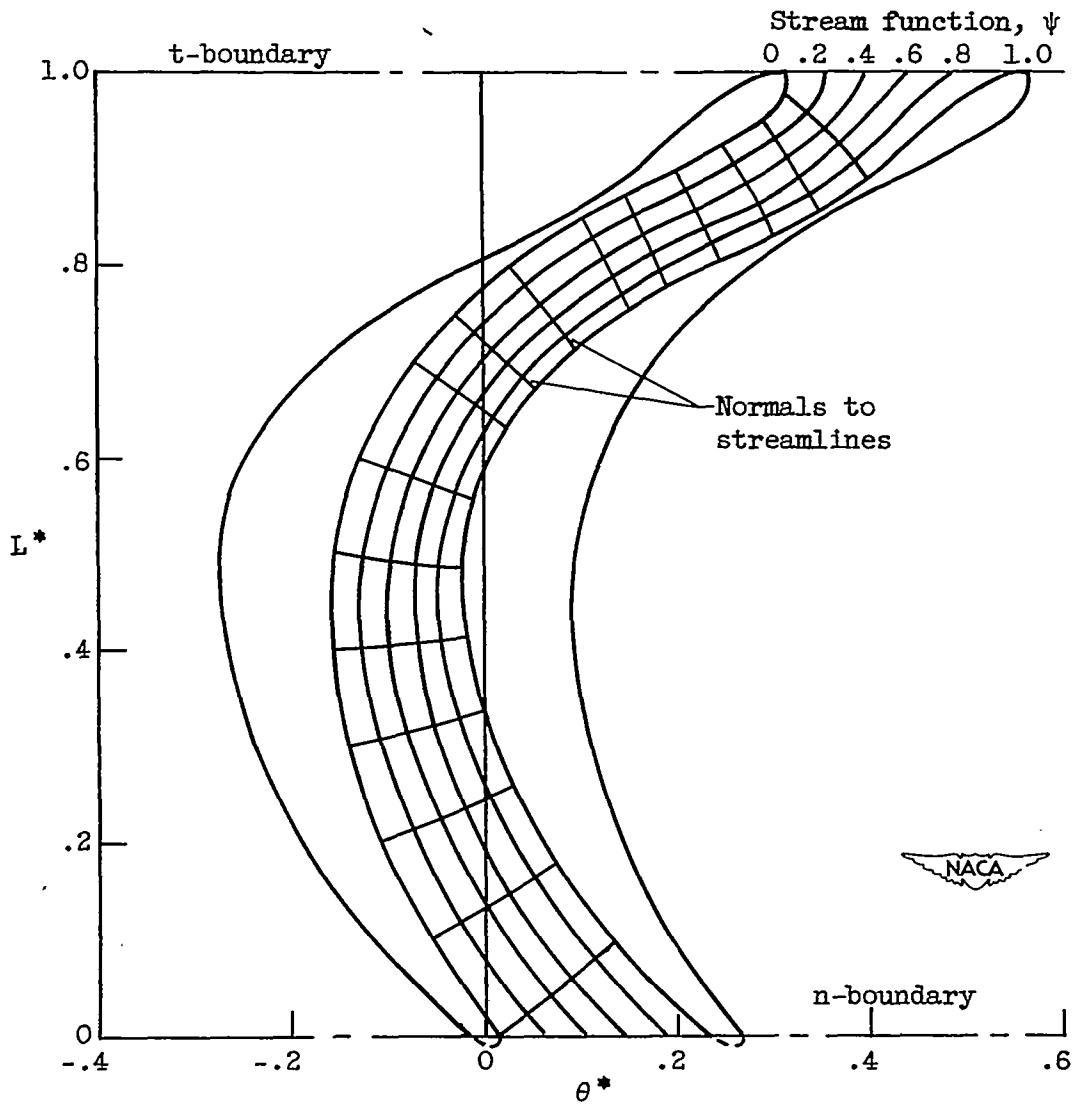

(b) Transformed $L^*\theta^*$-plane showing streamlines used in stream-filament check.

Figure 13. - Concluded. Blade-element profile for second numerical example.

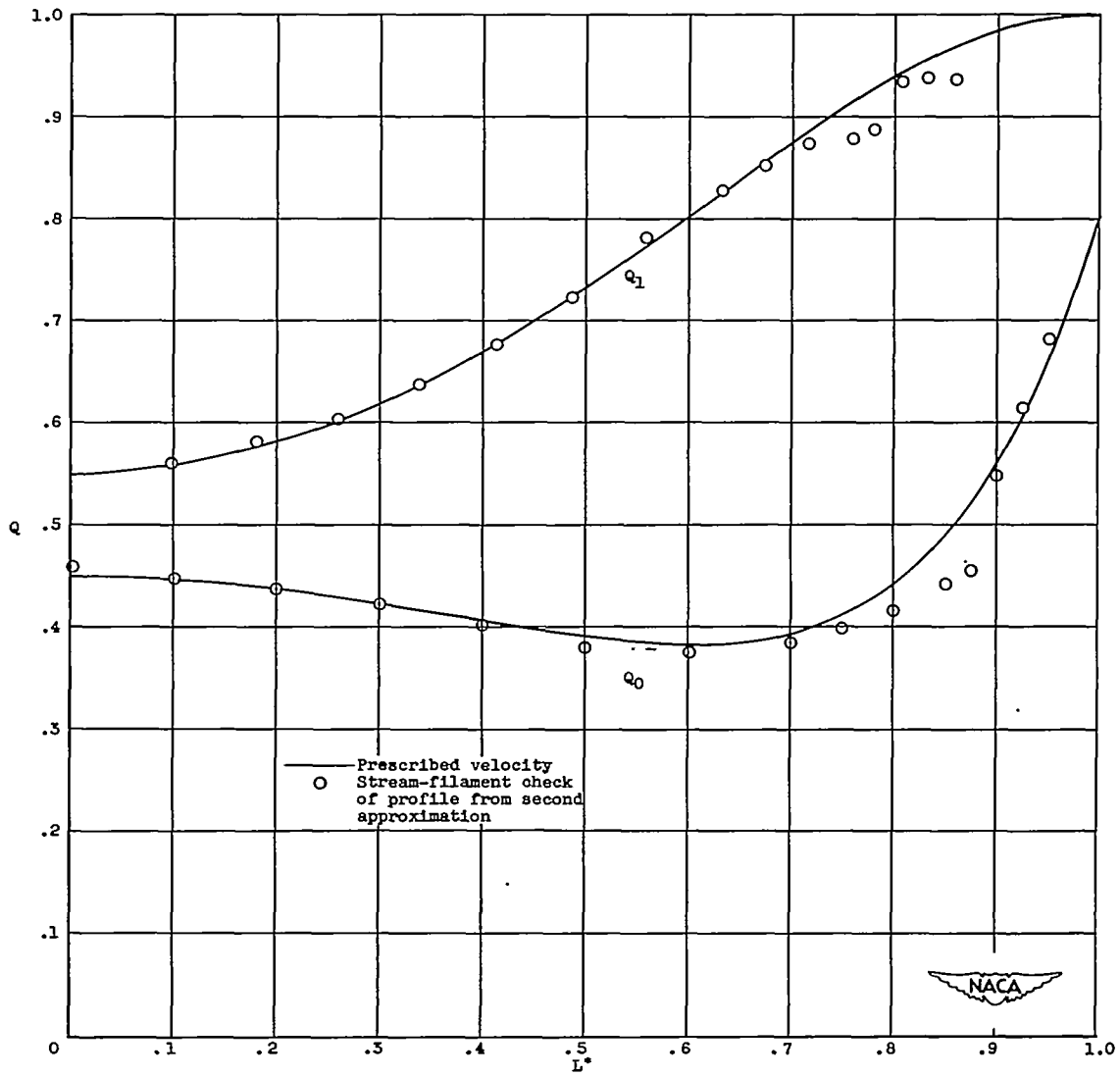

Figure 14. - Comparison of prescribed velocities for second numerical example with velocities obtained by stream-filament check of profile obtained by second approximation.

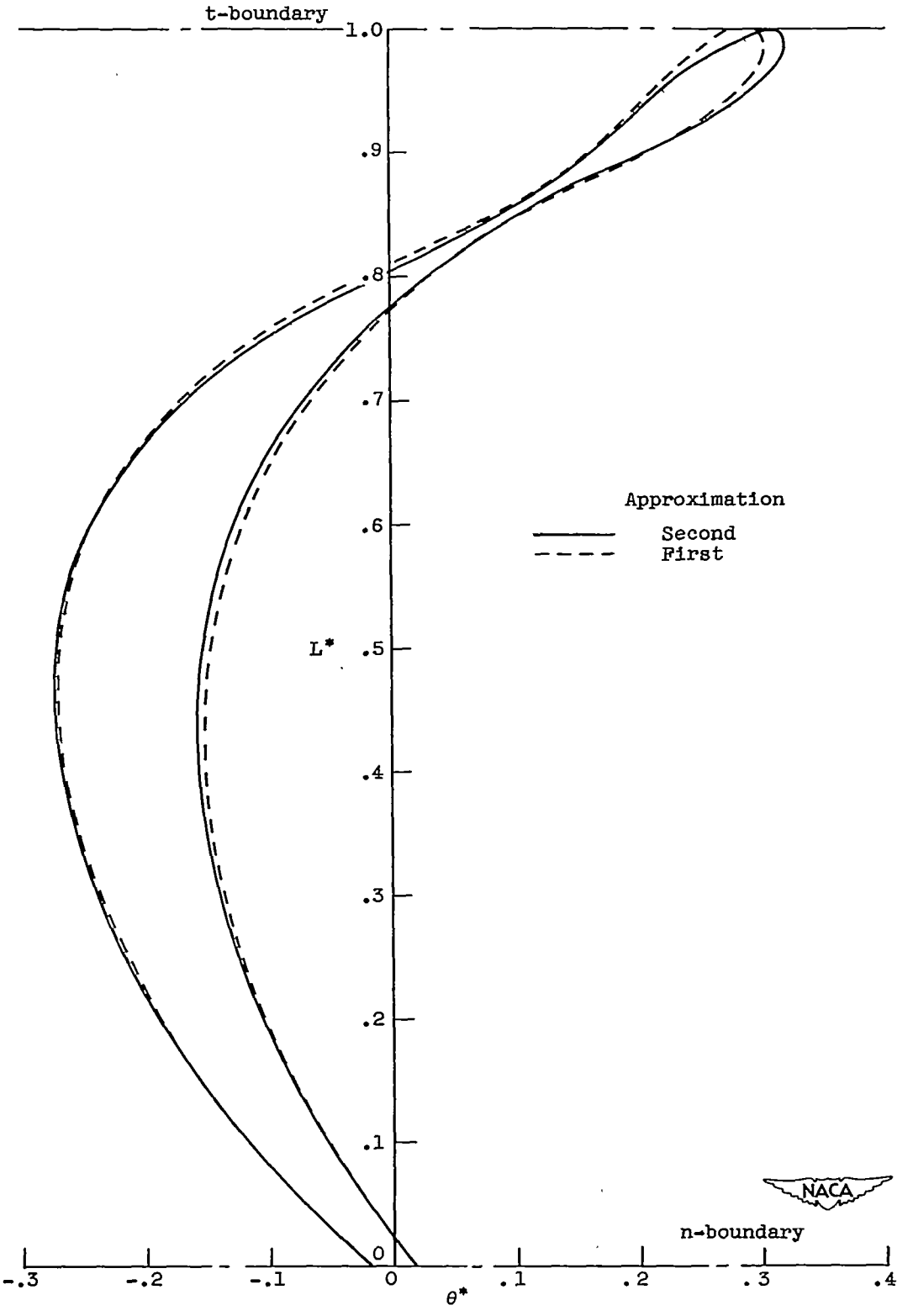

Figure 15. - Comparison of blade-element profiles obtained by first and second approximations for second numerical example.

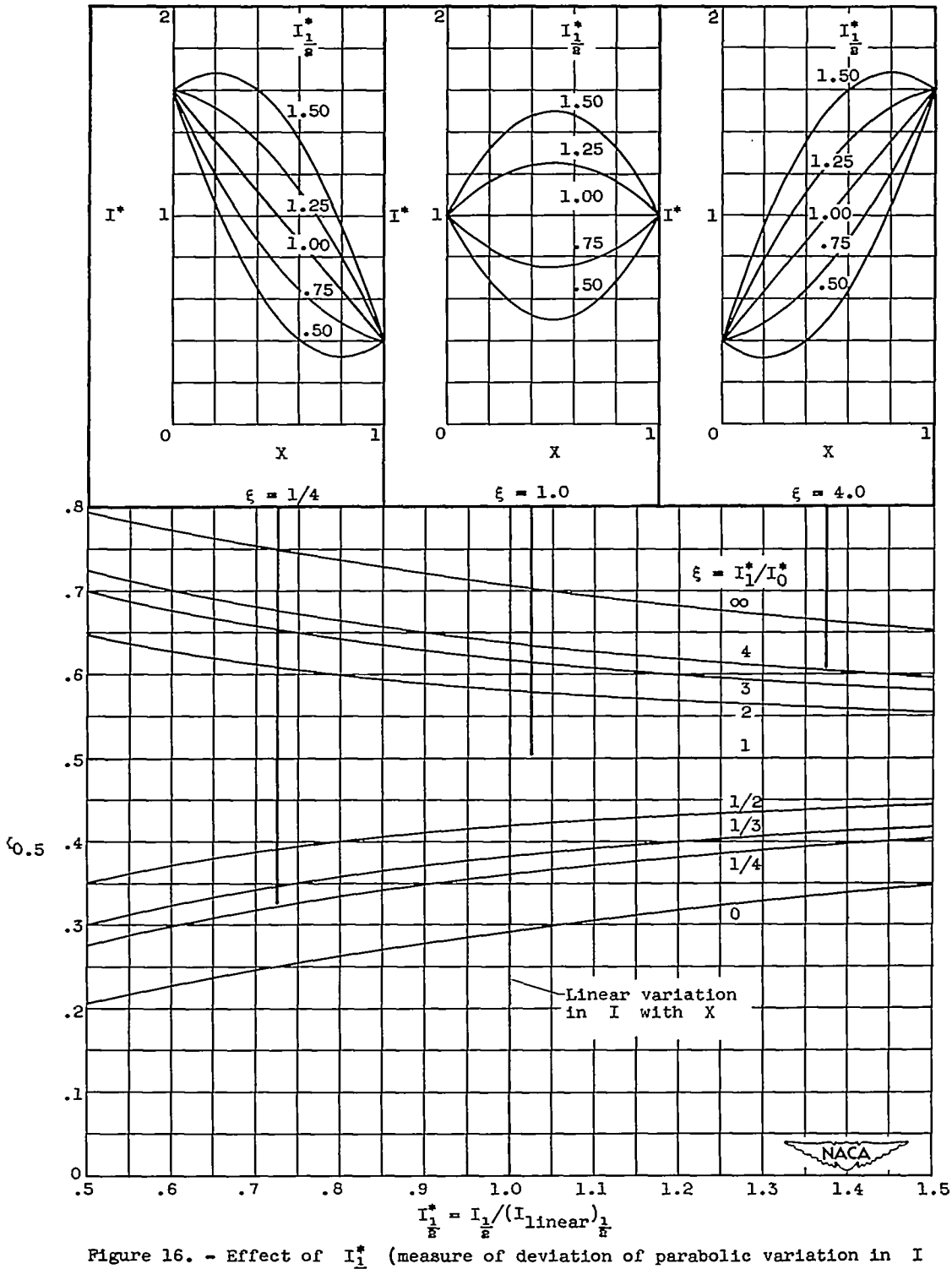

Figure 16. - Effect of $I^*_{\frac{1}{2}}$ (measure of deviation of parabolic variation in I from linear variation) and ξ (ratio of I^*_1 to I^*_0) upon ratio $X_{0.5}$.